Second ISSMGE R. Kerry Rowe Lecture: On the intrinsic, state, and fabric parameters of active clays for contaminant control

NRC Research Press

ARTICLE

Second ISSMGE R. Kerry Rowe Lecture: On the intrinsic, state, and fabric parameters of active clays for contaminant control

Mario Manassero

Abstract: The osmotic, hydraulic and self-healing efficiency of bentonite-based barriers for the containment of subsoil pollutants is governed not only by the intrinsic chemicophysical parameters of the bentonite, i.e., the solid phase density, ρ_{sk}; the total specific surface, S; the surface density of the electric charge, σ; and the Stern layer thickness, d_{Stern}, and fraction, f_{Stern}, but also by the chemicomechanical fabric parameters that quantify the structure or texture of the solid skeleton, such as the micro, e_m, and nano, e_n, void ratios; the average number of platelets or lamellae per tactoid, $N_{l,AV}$; and the solid skeleton effective electric charge concentration, $\bar{c}_{sk,0}$. In turn, the fabric parameters are controlled by state parameters, such as the total void ratio, e; and the salt concentration of the equilibrium solution, c_s. A theoretical framework has been developed to describe the relationships between the aforementioned intrinsic, state, and fabric parameters for a bentonite barrier and its performance parameters: the hydraulic conductivity, k; the effective diffusion coefficient, D_s^*; the chemico-osmotic efficiency coefficient, ω; and the osmotic swelling pressure, u_{sw}. The proposed theoretical hydrochemicomechanical model has been validated through comparison with a large amount of experimental results.

Key words: chemicohydromechanical behaviour, constitutive laws, geosynthetic clay liner, nuclear waste disposal, smectite fabric.

Résumé : L'efficacité osmotique, hydraulique et autocicatrisante des barrières à base de bentonite pour le confinement des polluants du sous-sol est non seulement régie par les paramètres chimicophysiques intrinsèques de la bentonite, tels que la densité de la phase solide, ρ_{sk}; la surface spécifique totale, S; la densité de surface de charge électrique, σ; et la couche de Stern par rapport à son épaisseur, d_{Stern}, et à sa fraction, f_{Stern}, mais aussi par les paramètres chimicomécaniques de tissu capables de quantifier la structure ou texture du squelette solide, tels que l'indice de vides à l'échelle micro, e_m, et nano, e_n; le nombre moyen de plaquettes ou lamelles par tactoide, $N_{l,AV}$; et la concentration effective de la charge électrique du squelette solide, $\bar{c}_{sk,0}$. À leur tour, les paramètres de tissu sont contrôlés par certains paramètres d'état, tels que l'indice de vides total, e, et la concentration de sel, c_s, dans la solution à l'équilibre. Un cadre théorique a été mis en place afin de décrire les relations entre les paramètres intrinsèques, d'état et de tissu mentionnés ci-dessus d'une barrière des polluants à base de bentonite avec ses paramètres de performance tels que la conductivité hydraulique, k; le coefficient de diffusion effectif, D_s^*; le coefficient d'efficacité osmotique, ω; et la pression de gonflement osmotique, u_{sw}. Le modèle hydrochimicomécanique théorique proposé a été validé par la comparaison avec un nombre considérable de résultats expérimentaux.

Mots-clés : comportement chimicohydromécanique, lois constitutives, revêtement d'argile géosynthétique, élimination de déchets nucléaires, tissu smectite.

Introduction

"Environmental geotechnics" pertains to a large variety of applications, such as the characterization of polluted sites and landfill waste, the design of containment systems for subsoil pollutant control, radioactive waste disposal, geo-energy exploitation, and bacteria-driven soil modification, among others. Nevertheless, the design of subsoil pollutant containment systems and the risk assessment associated with groundwater contamination from clay-lined landfills or the release of contaminants from canisters containing nuclear waste can be considered as among the foremost activities in environmental geotechnics from both fundamental research and related practical perspectives.

Many public institutions and private companies, worldwide, are currently investigating and assessing clayey media, such as bentonites, manmade compacted natural and (or) amended clays, and natural shales, for their possible use as engineered barriers for waste containment systems and (or) as host rocks of geologic repositories for "high level radioactive waste" (HLRW) (Andra 2005; Delay et al. 2007; Altmann 2008; Guyonnet et al. 2009; Bock et al. 2010; SKB 2011; Altmann et al. 2012; Shackelford and Moore 2013). In this regard, industrially produced sodium bentonites represent a favourable material for subsoil pollutant control as evidenced by their frequent use in manufactured geosynthetic clay liners (GCLs) used as barriers for landfill lining and capping systems, and as a buffer material around canisters hosting HLRW within underground repositories. Nevertheless, sodium bentonite is a highly sensitive material that is influenced to a great extent by several factors, including the intrinsic chemicophysical, state, and fabric parameters involving surface electrical charge, solid skeleton fabric, and related void volumes and ionic strength of pore fluids (Manassero 2017).

For typical applications involving GCLs, the bentonite within the GCL is usually at a low- to medium-density (void ratio, $e = 2–5$) and effective confining stress ($\sigma' = 10–1000$ kPa). In this condition,

Received 17 January 2019. Accepted 13 April 2019.

M. Manassero. Department of Structural, Geotechnical and Building Engineering, Politecnico di Torino, Corso Duca degli Abruzzi 24, 10129 Torino, Italy.
Email for correspondence: mario.manassero@polito.it.

both hydraulic conductivity, k, and diffusivity, D_s^*, can play significant roles in terms of pollutant transport. Moreover, other factors, such as the coupled fluxes of solvents and solutes, can greatly influence the barrier performance (Mitchell and Soga 2005).

In contrast, the conditions that generally exist at great depths where HLRW repositories are located, include very high densities (i.e., e = 0.2–1.0) and effective confining stress (σ' = 1000–10000 kPa). Under these conditions, bentonite-based barriers (e.g., buffers around canisters hosting HLRW) are characterized by negligible hydraulic conductivities, the ability to self-heal when fractured, and water and solute mass fluxes dominated by molecular diffusion (Leroy et al. 2006).

Based on the aforementioned considerations, the objectives of this paper are (*i*) to identify and quantify the intrinsic chemicophysical, state, and fabric parameters that govern the performance (i.e., hydraulic conductivity, diffusivity, osmotic efficiency, and osmotic swelling pressure) of bentonites when used as barriers for pollutant control, (*ii*) to link the aforementioned parameters within a theoretical model obtained by upscaling the modified Navier–Stokes and the Nernst–Planck equations and by using the Donnan equation and the imposition of the thermodynamic equilibrium between the bulk electrolyte solution and the internal micropore solution, (*iii*) to illustrate the use of the model to simulate the coupled fluxes of ions and water and the influence on bentonite stress–strain behaviour of the external actions in terms of both effective stress, pore pressure, and electrolyte concentration variations through a modified effective stress principle (Terzaghi 1936), and (*iv*) to establish a relationship within a three-dimensional (3D) domain linking electrolyte concentration, c_s; void ratio, e; and the average number of lamellae per tactoid, $N_{1,AV}$; with $N_{1,AV}$ being a newly introduced fundamental fabric parameter capable of describing and quantifying the lamellae arrangement in terms of texture or structure of bentonite.

The model is capable of simulating bentonite performance as a function of clay fabric, using the average number of platelets or lamellae per tactoid, $N_{1,AV}$; hydraulic conductivity, k; effective diffusion coefficient, D_s^*; osmotic efficiency, ω; and osmotic swelling pressure, u_{sw}; given a knowledge of the intrinsic and state input parameters. These intrinsic parameters include the solid phase density, ρ_{sk}; the surface density of electric charge, σ; the total specific surface, S; the average half distance between the platelets in the tactoid, b_n; the Stern layer thickness, d_{Stern}; and the related fraction coefficient, f_{Stern}. The state input parameters include the electrolyte concentration in the external solution, c_s, the ions electrochemical valence, z_i, and the void ratio, e.

Lastly, the proposed model is validated through comparison with the measurements of bentonite fabric arrangement using advanced techniques such as nuclear magnetic resonance (NMR), X-ray diffraction (XRD), small angle X-ray spectrometry (SAXS), and transmission electron microscopy (TEM). Moreover, further comparisons have been carried out through the assessment of bentonite fabric arrangement by the theoretical interpretation of experimental results from more traditional tests, such as hydraulic conductivity, osmotic swelling pressure, osmotic efficiency, and anion available pore volume tests, some of which have been conducted originally. For the sake of simplicity, the aforementioned advanced and traditional experimental techniques are referred to hereafter as "direct methods" and "indirect methods", respectively.

Bentonite components and fabric

Bentonite is a clayey soil that typically contains a significant percentage (e.g., >60%) of a high swelling smectite clay mineral, usually montmorillonite, with a 2:1 clay mineral structure comprising two sheets of silica tetrahedra that sandwich a central sheet of alumina octahedra (TOT). A more detailed description of the nature of the mineralogy and fabric of bentonite follows.

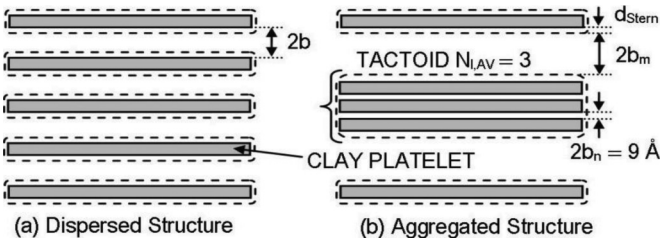

Fig. 1. Microscopic structure of clay soils containing montmorillonite as main mineralogical component: structure can be (*a*) dispersed if the lamellae of montmorillonite (or clay platelets) are present as individual units or (*b*) aggregated if the lamellae are condensed to form the so-called tactoids. $N_{l,AV}$, number of clay platelets per tactoid; b_m, half-distance of conducting pores; b_n, half distance of intra-tactoid pores containing immobile water; d_{Stern}, thickness of hydrated cations layer wrapping external tactoid surface.

Smectite lamellae

The formula of a smectite unit cell is $[(OH)_4Si_8Al_{3.34}Mg_{0.66}O_{20}\cdot nH_2O^{0.66-}]$, where n is the number of H_2O molecules interlayered between the TOT layers. As can be deduced from the previous formula, smectite carries an unbalanced negative electric charge because of isomorphic substitution of Si^{4+} by Al^{3+} in the silica tetrahedra and Al^{3+} by Fe^{2+} and (or) Mg^{2+} in the octahedral layer of the crystal lattice. Most of the isomorphic substitution occurs in the octahedral (gibbsite) sheet, whereas the substitution of Si^{4+} by Al^{3+} in the silica tetrahedra appears to be limited to less than about 15%. Grim (1962) notes that the substitution in the smectite lattice results in an average 0.66 net negative charge per unit cell.

Smectite crystals are organized in terms of parallel-aligned, aluminosilicate lamellae, which are approximately 1 nm thick and 100–200 nm in the lateral extent. The unit cell parameters are 0.517 and 0.895 nm, which correspond to a unit cell area of 0.925 nm², or one unit charge per 1.4 nm². The corresponding surface density of electric charge, σ, is equal to 0.114 C·m^{-2}. The total specific surface of a single platelet, S, available for water adsorption is approximately equal to 760 m^2·g^{-1}, assuming a solid phase density, ρ_{sk}, of 2.65 Mg·m^{-3} corresponding to a specific gravity of solids, G_s, of 2.65.

Smectite particles can be represented as infinitely extended platy particles, also called platelets or lamellae. Norrish (1954) showed that bentonite can have a dispersed structure or fabric in which clay particles are present as well-separated units or an aggregated structure that consists of packets of particles known as tactoids, within which several clay platelets are in a parallel array, with a characteristic interparticle distance of about 0.9 nm (Fig. 1).

Tactoid formation and bentonite fabric

The formation of tactoids has the net result of reducing the surface area of the montmorillonite, which then behaves as a much larger particle with the diffuse double layer (DDL) fully manifesting itself only on the outside surfaces. The formation of tactoids is due to internal flocculation of the clay platelets, and depends primarily on the concentration and valence of ions in the salt solution and, to a lesser extent, on the effective isotropic stress history or, in turn, the total void ratio, e. The average number of clay platelets or lamellae forming tactoids, $N_{l,AV}$, increases with an increase in the ion concentration and valence of cations in the salt solution. However, experimental evidence indicates no apparent unique trend in $N_{l,AV}$ versus the total void ratio e for a given concentration.

Referring to the parallel platelet array scheme (Fig. 1*a*), the average half-distance, b, in perfectly dispersed bentonites may be estimated (Dominijanni and Manassero 2012*b*) from the following relation:

$$(1) \qquad b = \frac{e}{\rho_{sk} S}$$

If the clay has an aggregated fabric or structure (Fig. 1*b*), then only the external surface of the tactoids can be assumed to interact with the mobile portion of the pore fluid and related ions in solution.

Therefore, if $N_{l,AV}$ is the average number of platelets per tactoid, the external or effective specific surface, S_{eff}, and the internal specific surface, S_n, are given as follows:

$$(2a) \qquad S_{eff} = \frac{S}{N_{l,AV}}$$

$$(2b) \qquad S_n = S - S_{eff} = \frac{(N_{l,AV} - 1)}{N_{l,AV}} S$$

Considering the previous scheme, with reference to the effective volume of the conducting pores (Manassero et al. 2016; Dominijanni et al. 2017), the thickness of the Stern layers, d_{Stern}, ranging between 1.2 and 2.0 nm and consisting of the first row of hydrated cations in direct contact with the negatively charged surface of the solid particles, can be taken into account. The hydrated cations of the Stern layer are characterized by a significantly reduced mobility (Tournassat et al. 2009; Muurinen et al. 2013; Shackelford and Moore 2013; Tinnacher et al. 2016) and, therefore, can be considered as a part of the solid phase with a consequent restriction of the microvoid space directly involved by the solvent and solute fluxes. Based on the previous assumptions and considerations, the void space within the platelets of the tactoids, together with the thickness of the hydrated cations in the Stern layer surrounding the external surface of the tactoid, should be subtracted from the total void space, e, to obtain the microvoid space, e_m, where almost the entire solute and solvent flow takes place. The average half distance between the platelets in the tactoid, b_n, as determined by means of X-ray measurements, can vary between 0.2 and 0.5 nm (Shainberg et al. 1971; Laird 2006).

In summary, the total void ratio, e, of the bentonite is given by the sum of the void ratio inside the tactoid, e_n, representing the nano or nonconductive pores (nm size), plus the volume occupied by the thickness of the Stern layers, and the void ratio representing the micro or conductive pores (μm size), e_m. The water inside the tactoids and the Stern layer can be considered as a portion of the solid particles and is excluded from any transport mechanisms.

Therefore, the void ratio associated with the internal surfaces of the tactoid and the hydrated cations of the Stern layer, e_n, can be estimated as follows:

$$(3) \qquad e_n = b_n \rho_{sk} \left(S_n + \frac{S d_d}{N_{l,AV}} \right)$$

where d_d is the thickness of the Stern layer consisting of hydrated cations wrapping the external surface of the tactoid, d_{Stern}, divided by the average half-distance between the platelets in the tactoid, b_n. Finally, the half-distance between the tactoids, in the case of an aggregate microstructure of bentonite, can be estimated in a similar manner to eq. (1) as follows:

$$(4) \qquad b_m = \frac{e_m}{\rho_{sk} S_{eff}}$$

where e_m (= $e - e_n$) is the void ratio representing the void space between the tactoids.

For a given total void ratio, e, when $d_d > 1$ and the number of clay platelets in the tactoids, $N_{l,AV}$, increases, the external specific surface decreases and the void ratio, e_m, representing the pore volume available for the solute and solvent transport, increases. In contrast, e_m decreases when $d_d < 1$ and, as in the previous case, $N_{l,AV}$ increases and the external specific surface decreases.

Guyonnet et al. (2005), through a comparison of the results of hydraulic conductivity tests and microscopic analyses of bentonite structure based on SAXS and TEM, showed that high hydraulic conductivity, k, is related to an aggregated fabric (also called the hydrated-solid phase), whereas low k is related to a dispersed fabric (also called the gel phase). These experimental results can be explained by the increase in the average micropore size, as well as the decrease in the seepage path tortuosity and in the effective specific surface, due to tactoid formation as discussed subsequently.

Chemicomechanical equilibrium conditions

An analysis of chemicomechanical equilibrium conditions is provided to separate partition effects, due to electric interactions between the ions in solutions and montmorillonite particles, from transport mechanisms, related to the motion of the different components of the pore solution. For the sake of simplicity, reference is made to the case of a pore solution containing a single salt, consisting of a cation (e.g., Na^+ or Ca^{2+}) and a common anion (e.g., Cl^-), assumed to be completely dissociated

$$(\text{Cation})^{\nu_c}_{z_c} (\text{Anion})^{\nu_a}_{z_a} \rightarrow \nu_c (\text{Cation})^{z_c} + \nu_a (\text{Anion})^{z_a}$$

where (ν_c, z_c) and (ν_a, z_a) are the stoichiometric coefficient and the electrochemical valence of the cation (index c) and the anion (index a), respectively.

The ionic concentrations, c_i (i = a, c), in the bulk solution are related to the salt concentration, c_s, as follows:

$$(5) \qquad c_i = \nu_i c_s$$

Equilibrium conditions and partition effect

If a porous medium is placed in contact with an external bulk solution, equilibrium is achieved after a sufficiently long time. At equilibrium and in the absence of partition mechanisms, the ion concentrations and the hydraulic pressure of the pore solution are equal to the ion concentrations and the hydraulic pressure of the external bulk solution. In contrast, this equality does not occur in the presence of partition mechanisms and a discontinuity in ion concentrations and hydraulic pressure between the external bulk solution and the pore solution occurs.

In bentonites, the primary partition mechanism is the electrostatic mechanism. At the macroscopic scale, this effect can be taken into account via Donnan's equations that define the equilibrium conditions between the pore solution of a charged porous medium and an external electrolyte solution. Donnan's equations establish the equality of the macroscopic electrochemical potentials between the components of the pore solution and the components of the external bulk solution, as follows:

$$(6a) \qquad \overline{\mu}_w = \mu_w$$

$$(6b) \qquad \overline{\mu}_i^{ec} = \mu_i^{ec} \qquad i = \text{a, c}$$

where $\overline{\mu}_w$ is the chemical potential of water in the pore solution (N·m·mol^{-1}), μ_w is the chemical potential of water in the external bulk solution (N·m·mol^{-1}), $\overline{\mu}_i^{ec}$ is the electrochemical potential of the ith ion in the pore solution (N·m·mol^{-1}), and μ_i^{ec} is the electrochemical potential of the ith ion in the external bulk solution (N·m·mol^{-1}).

Also, the following definitions of the electrochemical potentials, valid for dilute solutions, can be used to determine the relations between the pressure and the ion concentrations of the external bulk solution and the pore solution (Katchalsky and Curran 1965):

$$(7a)\qquad \begin{aligned}\mu_w &= \mu_w^0 + \frac{1}{c_w}(u - \Pi)\\ \overline{\mu}_w &= \overline{\mu}_w^0 + \frac{1}{\bar{c}_w}(\bar{u} - \overline{\Pi})\end{aligned}$$

$$(7b)\qquad \begin{aligned}\mu_i^{ec} &= \mu_i^0 + RT\ln(c_i) + z_iF\Phi\\ \overline{\mu}_i^{ec} &= \overline{\mu}_i^0 + RT\ln(\bar{c}_i) + z_iF\overline{\Phi}\end{aligned}$$

where μ_b^0 and $\overline{\mu}_b^0$ (for b = w, a, c) are constants of integration in the external and the pore solution, respectively (N·m·mol^{-1}); c_w and $\bar{c}_w$ are the water concentrations in the external and the pore solution, respectively; u and $\bar{u}$ are the fluid pressures in the external and the pore solution, respectively (Pa); c_i and $\bar{c}_i$ are the concentrations of the ith ion in the external and the pore solution, respectively (mol·m^{-3}); Φ and $\overline{\Phi}$ are the electric potentials in the external and the pore solution, respectively (V); $\Pi = RT\sum_{i=1}^{N_{ions}} c_i$ is the osmotic pressure in the external solution (Pa); $\overline{\Pi} = RT\sum_{i=1}^{N_{ions}} \bar{c}_i$ is the osmotic pressure in the pore solution (Pa); R is the universal gas constant (8.314 J·mol^{-1}·K^{-1}); T is the absolute temperature (K); and F is Faraday's constant (9.6485 × 10^4 C·mol^{-1}).

Assuming that $\mu_b^0 = \overline{\mu}_b^0$ (for b = w, a, c) and noting that the partition mechanism, based on the electrostatic interaction between the solid particles and the molecules in the pore solutions, acts only on the ion species and not on the electroneutral water molecules, such that $c_w = \bar{c}_w$, eqs. (7*a*) and (7*b*) can be expressed as follows:

$$(8)\qquad \bar{u} - \overline{\Pi} = u - \Pi$$

$$(9)\qquad \bar{c}_i = c_i\exp\left(-z_i\frac{F}{RT}\Psi\right)$$

where $\Psi = \overline{\Phi} - \Phi$ is the Donnan potential representing the characteristic electric potential of the solid skeleton.

An ion partition coefficient, Γ_i, can also be conveniently introduced as follows:

$$(10)\qquad \Gamma_i = \frac{\bar{c}_i}{c_i} = \exp\left(-z_i\frac{F}{RT}\Psi\right)$$

To close the system, the following equation, expressing the electroneutrality condition within the pore solution, is required:

$$(11)\qquad \sum z_i\bar{c}_i = \frac{\bar{c}_{sk,0}}{e_m}$$

where $\bar{c}_{sk,0}$ is solid skeleton effective electric charge concentration within pore solution (mol·m^{-3}).

In the case of a solution containing a (1:1) electrolyte (e.g., NaCl or KCl), the ion partition coefficients are given by

$$(12)\qquad \Gamma_a = \Gamma_c^{-1} = -\frac{\xi}{2} + \sqrt{\left(\frac{\xi}{2}\right)^2 + 1}$$

where $\xi = \bar{c}_{sk,0}/e_m c_s$

The coefficient $\Gamma_c \geq 1$ describes the accumulation of the cations within bentonite pores, whereas $0 \leq \Gamma_a \leq 1$ describes the exclusion of the anions. When $\Gamma_c = \Gamma_a = 1$, bentonite does not generate a partition of the ions and has no selective capability. When $\Gamma_a = 0$ and $\Gamma_c \to \infty$, the membrane is "ideal" or "perfect", such that the passage of the salt is restricted completely.

The term $\bar{c}_{sk,0}$ can be estimated on the basis of an idealized model for bentonite fabric. Bentonite can display a hierarchy of structures that are referred to as lamellae at the finest level; tactoids, quasi-crystals or particles at the microscopic level; mesoaggregate or cluster at the mesoscopic level; and macroaggregates or peds on the macroscopic scale (Quirk and Aylmore 1971; Guyonnet et al. 2005; Shackelford and Moore 2013; Acikel et al. 2018). A low k (<10^{-9} m·s^{-1}) is compatible only with the absence of meso and macro aggregates. If the tactoids are assumed to be formed by packets of parallel lamellae (platelets) such that the only mobile fraction of the pore solution is the one located in the intertactoids pore space, while the pore solution within the tactoids is considered as part of the solid phase, then $\bar{c}_{sk,0}$ can be estimated as follows (Dominijanni and Manassero 2008, 2012*a*, 2012*b*; Dominijanni et al. 2013):

$$(13)\qquad \bar{c}_{sk,0} = \frac{(1 - f_{Stern})\sigma\rho_{sk}S_{eff}}{F}$$

where f_{Stern} is the fraction of electric charge compensated by the cations specifically adsorbed in the Stern layer, σ is the surface density of the electric charge (C·m^{-2}), ρ_{sk} is the density of the solid phase (g·m^{-3}), and S_{eff} is the effective specific surface of tactoids (m^2·g^{-1}).

Osmotic swelling pressure

Under the assumption of elastic behaviour of the solid skeleton (no free energy dissipation during the deformation processes) and very small area of the intertactoid contacts in comparison with the total area of a generic cross section of the soil (Skempton 1961), the intertactoid stress can be defined directly at the macroscopic scale without having to employ an upscaling procedure, such that the intergranular or effective confining stress, σ', for bentonite can be expressed as follows in the case of an electrically charged soil surface that is in contact with a single electrolyte solution (Dominijanni and Manassero 2008; Musso et al. 2017):

$$(14)\qquad \sigma' = \sigma - \bar{u} = \sigma - u - \underbrace{(\overline{\Pi} - \Pi)}_{u_{sw}}$$

where

$$(15)\qquad u_{sw} = 2RTc_s\left[\sqrt{(\xi)^2 + 1} - 1\right]$$

The term u_{sw}, which is a function of $\bar{c}_{sk,0}$, c_s, and e_m through eqs. (8) and (12), represents the osmotic swelling pressure. When the salt concentration increases, the osmotic swelling pressure decreases up to negligible values. Thus, higher values of osmotic swelling pressure are associated with higher values of $\bar{c}_{sk,0}$. At low salt concentrations, the osmotic swelling pressure tends to the theoretical maximum value, given as $u_{sw} = RT\bar{c}_{sk,0}/e_m$.

Taking the oedometric conditions into consideration and based on the previous assumptions, and more specifically at the volumetric rigidity under the external actions of the tactoids (i.e., $de_n = 0$), the microvoid ratio, e_m, of the surface charged soil is related to the effective stresses as follows:

$$(16)\qquad e_m = e_{m,0} - a_v(\sigma' - \sigma_0')$$

where $e_{m,0}$ is the void ratio at a reference state, a_v is the bentonite compressibility of intergranular contacts (Pa^{-1}), and σ_0' is the ef-

Fig. 2. Mechanical model of charged porous medium. A, cross-sectional area of the porous medium; u, hydraulic pressure in the external bulk solution; u_{sw}, chemico-osmotic swelling pressure; σ, total vertical stress; σ', effective vertical stress.

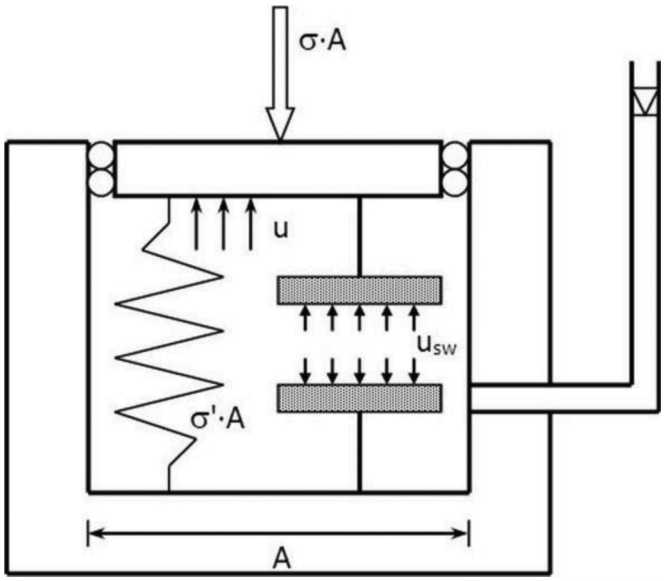

fective stress at a reference state (1 Pa). Using eqs. (14) and (15), the void ratio is related not only to the apparent effective stress σ'_{app} ($= \sigma - u$), but also to the chemical composition and ion concentration of the pore solution through the osmotic swelling pressure, u_{sw}.

High salt concentration and substitution of divalent for monovalent cations result in a reduction in the osmotic swelling pressure and a consequent increase in the effective stress. Such an increase in the effective stress results in compression of bentonite, i.e., a reduction in the void ratio, a process referred to as "chemical consolidation" (Kaczmarek and Hueckel 1998).

However, local increase in the effective stress at the microscopic scale can promote aggregation of montmorillonite lamellae, causing the formation of thicker tactoids. The increase in the number of lamellae per tactoid determines a reduction in S_{eff}, and a possible increase in the intergranular contact resulting in a decrease in the compressibility, a_v. At the macroscopic scale, such modifications in bentonite fabric result in an enhancement of mechanical characteristics, such as rigidity and shear strength, and a degradation of barrier properties (i.e., an increase in k). This last effect is of particular concern for environmental applications.

In bentonite characterized by a very high void ratio, as in the case of bentonite suspensions, a lack of contacts between solid particles can be assumed such that effective stresses can be considered nil. Such an assumption has been made, for instance, by Bolt (1956) and is equivalent to assuming $d\sigma' = 0$ or $a_v \rightarrow \infty$.

As far as Terzaghi's effective stress principle for soils is concerned, a simple modification is sufficient to model the mechanical behaviour of a charged porous medium, such as bentonite. In fact, the osmotic swelling pressure can be taken into account by a second effect representing the interaction of repulsive forces by the solid particles at the microscopic scale. From Fig. 2 and eq. (14), equilibrium with external forces can also be reached in the absence of the spring representing the intergranular contacts.

An interesting development related to eq. (16) can be obtained by a differentiation and re-formulation as follows:

$$(17) \qquad d\varepsilon_v = \frac{a_v}{1 + e_{m,0}} d(\sigma - u - u_{sw}) = \frac{-de_m}{1 + e_{m,0}}$$

where ε_v represents the volumetric strain. The development of the stress component differentiations gives

$$(18) \qquad d(\sigma - u - u_{sw}) = d(\sigma - u) - \frac{du_{sw}}{de_m} de_m - \frac{du_{sw}}{d\Pi} d\Pi$$

and, therefore, the microvoid ratio variation, de_m, can be expressed as a function of the apparent effective stress, $\sigma - u$; the osmotic swelling pressure, u_{sw}; the salt concentration, c_s; and the solid skeleton effective electric charge concentration, $\bar{c}_{sk,0}$; or

$$(19) \qquad de_m = -\frac{a_v a_\pi}{a_v + a_\pi} [d(\sigma - u) + \varpi d\Pi]$$

where

$$\varpi = 1 - \frac{1}{\sqrt{\left(\frac{\xi}{2}\right)^2 + 1}} \qquad a_\pi = \frac{2c_s e_m^3 \sqrt{\left(\frac{\xi}{2}\right)^2 + 1}}{RT\bar{c}_{sk,0}^2} \qquad \Pi = 2RTc_s$$

An interesting observation is that further integration of eq. (19) represents the fundamental fabric boundary surface (FBS) of the chemicomechanical behaviour of the bentonite (Figs. 3*a*, 3*b*, and 3*c*), because the result links the external salt concentration, c_s, the microvoid ratio, e_m, and the average number of lamellae per tactoid, $N_{l,AV}$, which is inversely proportional to $\bar{c}_{sk,0}$ that, in turn, is linked directly to the Faraday constant, F, and to the intrinsic parameters including the surface density of electric charge, σ; the total specific surface of the basic lamellae, S; and the solid phase density, ρ_{sk}; of the bentonite.

Moreover, the remaining input intrinsic parameters to be taken into account, i.e., the average half-distance between two platelets in the tactoid, b_n (ranging from 0.8 to 1.0 nm); the Stern fraction, f_{Stern} (ranging from 0.70 to 0.95); and the thickness, d_{Stern} (ranging from 1.2 to 2.0 nm); are characterized by a narrow range of variation that can be assessed and used without significant reliability problems for current predictions. In contrast, these parameters can also allow a further calibration of the model input data for interpretation of experimental results.

The range of validity of eq. (19) in representing the FBS of the bentonite is limited to microvoid size and related distances between tactoids that are significantly greater than the nano void size and related distances between the platelets of the same tactoid. This limitation occurs because, when the dispersed platelets reach the critical distance corresponding to the van der Waals attraction overcoming the electrostatic repulsion, e.g., under exceptionally high confining effective stresses, tactoid formation occurs also in the presence of very low electrolyte concentrations such as deionized water (i.e., a solution having a null salt concentration, $c_s = 0$) and this phenomenon is not taken into account by eq. (19). Thus, the consequent change of the e_m versus $N_{l,AV}$ trend, i.e., the increase in the number of lamellae per tactoid when e_m decreases down to $e_m = 0$, cannot be represented by eq. (19).

Moreover, note that appropriate boundary conditions have been used for obtaining the best fit, by integration of eq. (19), of the leading group of experimental results that will be illustrated subsequently. The FBS obtained is shown in Figs. 3*a*, 3*b*, and 3*c*.

Unfortunately, the integration of eq. (19) is complex and cannot be solved in a closed form. Therefore, as shown subsequently, an approximate solution has been formulated (Figs. 3*d*, 3*e*, and 3*f*) to facilitate an efficient use of the proposed model, particularly with respect to the aforementioned change in the trend of e_m versus $N_{l,AV}$ at extremely high effective confining stresses and correspondingly very small total void ratio (Fig. 3*d*).

Fig. 3. Fabric boundary surface (FBS): (*a*, *b*, *c*) theoretical derivation; (*d*, *e*, *f*) operative simplified version.

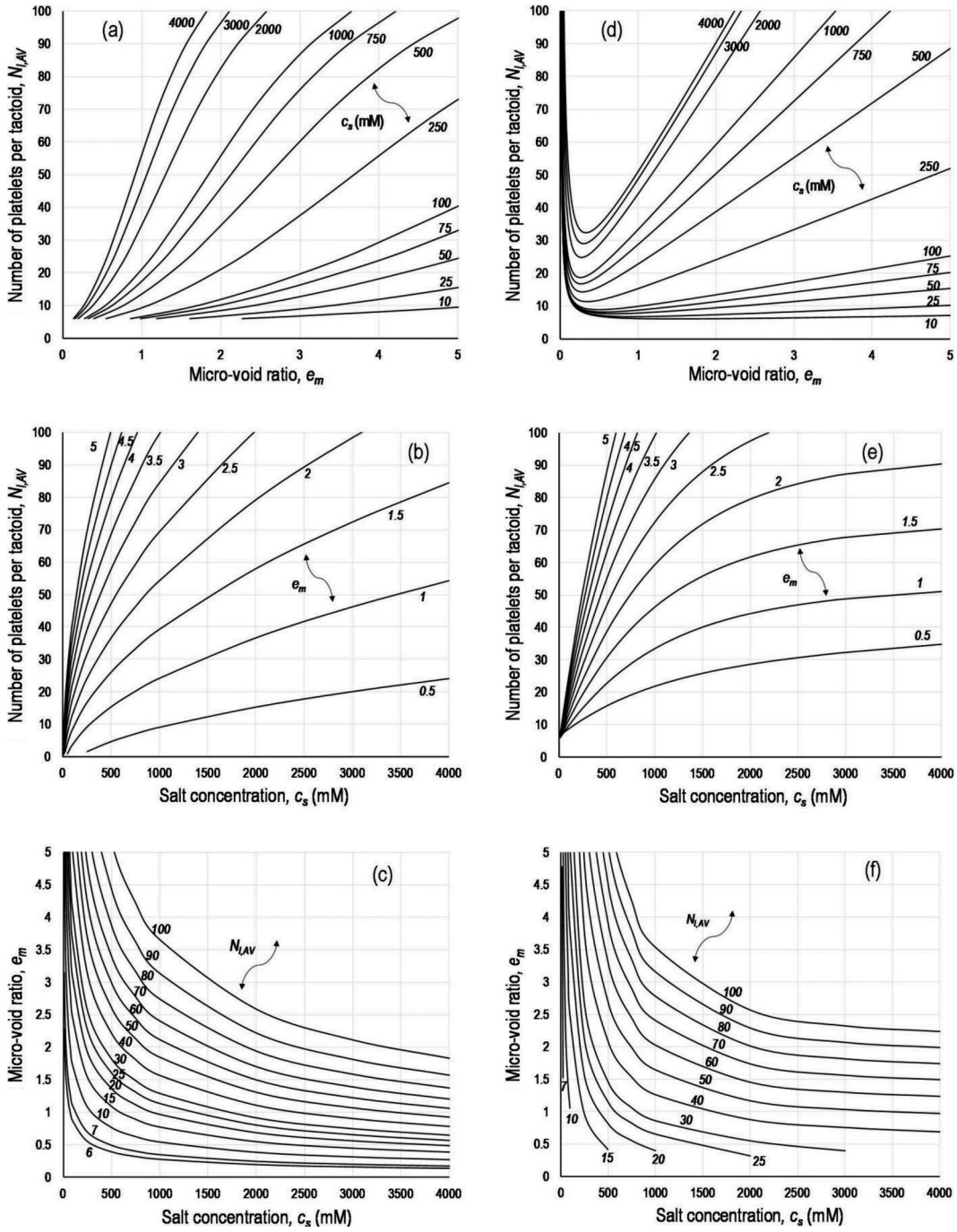

Coupled fluxes and transport

In the case of the most general approach to model the coupled fluxes in porous media, invoking the phenomenological equations, based on the thermodynamics of irreversible processes, is convenient (Katchalsky and Curran 1965; Yaroshchuk 1995; Manassero and Dominijanni 2003). The primary advantage of this approach is to avoid any specification of physical properties of the membrane, maintaining the model as general as possible. Using such a formalism, Spiegler and Kedem (1966) derived the following equations for a semi-permeable membrane permeated by a solution containing a single salt (e.g., NaCl, KCl or $CaCl_2$):

$$q = -P_{v\lambda}\left(\frac{du}{dx} - \omega_\lambda \frac{d\Pi}{dx}\right) \tag{20}$$

$$J_s = (1 - \omega_\lambda)qc_s - P_{s\lambda}\frac{dc_s}{dx} \tag{21}$$

where q is the volumetric solution flux ($m^3 \cdot m^{-2} \cdot s^{-1}$), J_s is the salt mass flux ($mol \cdot m^{-2} \cdot s^{-1}$), and $\Pi = (\nu_a + \nu_c)RTc_s$ is the virtual osmotic pressure ($N \cdot m^{-2}$). In eqs. (20) and (21), there are three phenomenological coefficients, viz., (*i*) $P_{v\lambda}$ is the specific hydraulic conductivity ($m^4 \cdot s^{-1} \cdot N^{-1}$), (*ii*) ω_λ is the local chemico-osmotic efficiency coefficient, and (*iii*) $P_{s\lambda}$ is the local salt permeability ($m^{-2} \cdot s$). The state variables are the virtual hydraulic pressure, u; and the virtual salt concentration, c_s; which represent, respectively, the pressure and the salt concentration of a virtual external bulk solution that is assumed to be in thermodynamic equilibrium with the

pore solution in correspondence to a given volume element of the porous medium. Virtual variables can be used to avoid the introduction of any physical assumption on the formulation of flux equations. At the boundaries, the virtual solution coincides with the real bulk solution in contact with the porous medium. Therefore, the steady-state solutions of eqs. (20) and (21) can be expressed using the pressure and the salt concentration of the bulk solutions in contact with the bentonite barrier as boundary conditions. Also, the phenomenological coefficients $P_{v\lambda}$, ω_λ, and $P_{s\lambda}$ are unspecified functions of the salt concentration, c_s; and the hydraulic pressure, u (or the void ratio, e_m).

The specific hydraulic conductivity can be expressed in terms of the more common local hydraulic conductivity, k_λ, as follows:

$$P_{v\lambda} = \frac{k_\lambda}{\gamma_w} \tag{22}$$

where γ_w is the water unit weight (N·m^{-3}).

Based on this approach, all the phenomenological coefficients can be measured by means of suitable tests, without any assumption about their relation to physical properties of the bentonite barrier. However, the experimental determination of these parameters is particularly difficult due to their dependency on the salt concentration.

By linearizing the flux equations (eqs. (20) and (21)), analytical solutions at steady-state conditions can be obtained as follows:

$$q = \frac{k}{\gamma_w}\left(\frac{\Delta u}{L} - \omega\frac{\Delta \Pi}{L}\right) \tag{23}$$

$$J_s = (1 - \omega)q\frac{c_s' \exp(P_{L\pi}) - c_s''}{\exp(P_{L\pi}) - 1} \tag{24}$$

where

$$P_{L\pi} = \frac{(1 - \omega)qL}{P_s} \tag{25}$$

Δu and $\Delta \Pi$ are the differences in hydraulic and osmotic pressure across the porous medium, respectively; L is the length of the barrier; c_s' and c_s'' represent the salt concentrations of the external bulk solutions in contact with the barrier at the boundaries; and P_s is the global value of the local salt permeability (as defined below by eq. (28)).

In eqs. (23)–(25), the global coefficients k, ω, and P_s are average values of the respective local coefficients, or

$$k = \frac{1}{L}\int_0^L k_\lambda\, dx \cong \frac{1}{\Delta c_s}\int_{c_s'}^{c_s''} k_\lambda\, dc_s \tag{26}$$

$$\omega = \frac{1}{L}\int_0^L \omega_\lambda\, dx \cong \frac{1}{\Delta c_s}\int_{c_s'}^{c_s''} \omega_\lambda\, dc_s \tag{27}$$

$$P_s = \frac{1}{L}\int_0^L P_{s\lambda}\, dx \cong \frac{1}{\Delta c_s}\int_{c_s'}^{c_s''} P_{s\lambda}\, dc_s \tag{28}$$

where $\Delta c_s = c_s' - c_s''$.

To obtain an understanding of the physical meaning of the phenomenological coefficients, although limiting the generality of the approach, Dominijanni and Manassero (2005), Dominijanni et al. (2006), Manassero and Dominijanni (2010), and Manassero et al. (2014) proposed a model obtained by upscaling the modified Navier–Stokes equation and the Nernst–Planck equations and using Donnan's equations to express the relations between real and virtual variables. The proposed model provides an interpretation of the experimental results of Malusis and Shackelford (2002*a*, 2002*b*), Malusis et al. (2013), Dominijanni et al. (2013), and Shackelford et al. (2016). Based on the theoretical and experimental findings, the following observations were made.

First, the hydraulic conductivity, k_λ, corresponding to relatively low values of the salt concentration (≤10^{-1} mol·L^{-1}), is dependent on the salt concentration due to the electroviscous effect and can be expressed as follows:

$$k_\lambda = \frac{\tau_m}{3}\frac{e_m^3}{(1 + e_m)}\frac{\gamma_w}{(\rho_{sk}S_{eff})^2}\frac{1}{\mu_e(c_s', c_s'', \bar{c}_{sk,0})} \tag{29}$$

where τ_m is the matrix tortuosity factor (≤1) that takes into account the tortuous nature of the actual migration pathways through the porous medium due to the geometry of the interconnected pores and μ_e is the electroviscous coefficient, which is related to the boundary salt concentrations c_s', c_s'' and the solid skeleton effective electric charge concentration, $\bar{c}_{sk,0}$. The τ_m for bentonites can be estimated, as a first approximation, referring to a range on the order of 0.1–0.3 (see Kato et al. 1995; Ichikawa et al. 2004; Bourg et al. 2006). Moreover, if the electroviscous effect is neglected, the electroviscous coefficient can be considered almost equal to the viscous coefficient of water, μ_w, and, as a first approximation, $k_\lambda \cong k \cong$ constant can be assumed.

Second, the chemico-osmotic efficiency, ω, for a (1:1) electrolyte (e.g., NaCl or KCl) can be expressed as follows (Dominijanni et al. 2018):

$$\omega = 1 + \frac{\bar{c}_{sk,0}}{2\Delta c_s e_m}\left[Z_2 - Z_1 - (2t_c - 1)\ln\left(\frac{Z_2 + 2t_c - 1}{Z_1 + 2t_c - 1}\right)\right] \tag{30}$$

where

$$Z_1 = \sqrt{1 + \left[2c_s'(e_m/\bar{c}_{sk,0})\right]^2} \qquad Z_2 = \sqrt{1 + \left[2c_s''(e_m/\bar{c}_{sk,0})\right]^2} \tag{31}$$

t_c is the cation transport number

$$t_c = \frac{D_{0c}}{D_{0c} + D_{0a}} \tag{32}$$

D_{0c} is the cation free-solution diffusion coefficient (m^2·s^{-1}) and D_{0a} is the anion free-solution diffusion coefficient (m^2·s^{-1}).

Third, the salt permeability can be expressed as follows:

$$P_s = (1 - \omega)nD_s^* = nD_\omega^* \tag{33}$$

where D_ω^* is the global effective osmotic diffusion coefficient and D_s^* is the effective diffusion coefficient of the salt (m^2·s^{-1}), given by

$$D_s^* = \tau_m\frac{(\nu_c + \nu_a)D_{0c}D_{0a}}{\nu_a D_{0c} + \nu_c D_{0a}} \tag{34}$$

Note that when $\bar{c}_{sk,0} \to 0$, $\omega \to 0$ such that the flux eqs. (23) and (24) reduce to the expressions of the basic advective-diffusive transport theory.

Table 1. Selected chemico-physical intrinsic parameters for GCLs bentonites tested by Malusis and Shackelford (2002*a*, 2002*b*), Dominijanni et al. (2013), and Shackelford et al. (2016).

	Bentomat	GeobentXP
Liquid limit, LL (%)	478	525
Plasticity index, PI (%)	439	—
Specific gravity, G_s	2.43–2.68	2.65
Principal minerals (%):		
Montmorillonite	71	98
Mixed-layer illite–smectite	7	—
Quartz	15	—
Other	7	—
Cation exchange capacity, CEC (meq/100 g)	47.7	105

Table 2. State, fabric, and performance parameters of GCL bentonites derived from interpretation of (*a*) Malusis and Shackelford (2002*a*, 2002*b*) and Shackelford et al. (2016) and (*b*) Dominijanni et al. (2013).

Parameter	(*a*)	(*b*)
Hydraulic conductivity, k ($m \cdot s^{-1}$)	9.00×10^{-12}	8.00×10^{-12}
	1.63×10^{-11}	—
Porosity, n	0.79	0.81
Void ratio, e	3.76	4.26
Effective diffusion coefficient, D_s^* ($m^2 \cdot s^{-1}$)	1.5×10^{-10}	5.0×10^{-10}
	2.7×10^{-10}	—
Thickness, L (mm)	8	17
	10	—
Solid skeleton effective electric charge concentration, $\bar{c}_{sk,0}$ ($mol \cdot L^{-1}$)	0.033	0.090
	0.015	—

Preliminary comparison of experimental and theoretical results

The initial part of the proposed theoretical model described previously has been validated using a first series of experimental results reported in Malusis and Shackelford (2002*a*, 2002*b*), Malusis et al. (2013), Dominijanni et al. (2013), and Shackelford et al. (2016). The experimental results were obtained by carrying out basically two kinds of tests, viz., (*i*) osmotic swelling pressure tests and (*ii*) chemico-osmotic diffusive tests, and by using bentonites from two different GCLs, whose basic characteristics are reported in Table 1. Potassium chloride (KCl) solutions at different concentrations were used by Malusis and Shackelford (2002*a*, 2002*b*), Malusis et al. (2013), and Shackelford et al. (2016); whereas, Dominijanni et al. (2013) used a sodium chloride (NaCl) as the salt.

The osmotic swelling pressure tests conducted by Dominijanni et al. (2013) used an apparatus consisting of a stainless steel oedometer cell; a NaCl solution supply tank placed above a pressure panel board; a displacement transducer connected to the cell top piston, which is used to measure the axial strains of the specimen; a load cell; and a data acquisition system. The sample is confined by a rigid cell, which allows access to the water through both porous stones. The cell is connected to a pressure panel board that allows the specimen to be back-pressured. The rigid piston above the upper porous stone is connected to the load cell, which measures the pressure that must be applied to hinder the axial strain of the specimen.

The test procedure requires a known amount of dry material to be dusted inside the oedometer ring, the cell to be assembled, and a NaCl solution to be supplied. The specimen, which is characterized by an initial dry height of 5 mm, is allowed to swell to 10 mm. The piston is then blocked, the sample is back-pressurized, and the steady-state swelling pressure is recorded after a short transitional phase. As the bentonite that is initially dusted inside the oedometer is dry, the pressure increases for a number of days during the hydration phase, and then the steady-state swelling pressure is reached when hydration has been completed.

The chemico-osmotic diffusive test apparatus used in all the aforementioned studies to measure the salt permeability, P_s (also defined, in the related literature, as the product of global osmotic effective diffusion coefficient, D_ω^*, times the porosity, n) is described in detail in Malusis et al. (2001).

The primary components of the apparatus are the osmotic cell, the flow pump system, and the pressure transducer, which is used to measure the differential pressure that develops across the specimen during the test. The cell consists of a modified rigid-wall permeameter, in which the top piston and the bottom pedestal are equipped with three ports each, with two ports enabling the different solutions to circulate through the top (e.g., NaCl or KCl solution) and through the bottom (e.g., deionized water) porous stones, to establish a constant concentration gradient across the specimen. The third port is installed in both the top piston and the bottom pedestal to allow the differential pressure across the specimen to be measured. The flow pump system, which consists of a dual-carriage syringe pump and two stainless steel accumulators (actuators), prevents any volumetric flux through the specimen by simultaneously injecting into and withdrawing from the porous stones the same volume of solution. To obtain this result, the syringes must displace the liquids across the top and bottom of the specimen at the same rate. All the tests were performed according to the procedure proposed by Malusis et al. (2001), whereby a solution containing a known electrolyte concentration (KCl or NaCl) was circulated in the top porous stone, while deionized water was circulated in the bottom porous stone. The concentration difference across the specimen was maintained constant by continuously infusing the two liquids at the boundaries of the specimen.

The interpretation of the previously illustrated series of tests is summarized in Table 2 in terms of the primary chemicophysical parameters that can be used to evaluate the bentonite barrier performance, including the osmotic effect (among others). Moreover, based on the proposed theoretical model, both the osmotic swelling pressure, u_{sw}, and the chemico-osmotic efficiency, ω, depend, particularly at low concentration, c_s, on the solid skeleton effective electric charge concentration, $\bar{c}_{sk,0}$, through eqs. (15) and (30). Therefore, by regressing the theoretical curves with the experimental data for both the swelling and chemico-osmotic efficiency tests reported by Dominijanni et al. (2013), an average value of $\bar{c}_{sk,0}$ equal to 0.09 $mol \cdot L^{-1}$ was determined. The obtained theoretical curves are shown in Figs. 4 and 5 together with the experimental data. The resulting agreement between theoretical and experimental data is good, especially when considering that, through the calibration of only one average parameter (i.e., the solid skeleton effective electric charge concentration, $\bar{c}_{sk,0}$), reliable interpretations of very different types of tests (i.e., swelling and chemo-osmotic diffusion), involving both stress–strain behaviour and transport phenomena that occur within very complex systems such as bentonite minerals with related pore fluids and electrolytes in solution, were possible.

Nevertheless, the most significant experimental data for determining the fitting parameters for the theoretical functions are those at the lowest concentrations and at the highest osmotic swelling pressure and osmotic efficiency, because both of the aforementioned properties tend to disappear regardless of the values of $\bar{c}_{sk,0}$ and, consequently, $N_{1,AV}$ at the highest concentrations.

For this reason, the experimental data from Shackelford et al. (2016), characterized by high c_s and low ω, are shown in Fig. 5 together with the range of $N_{1,AV}$ values used for obtaining each experimental result from the lowest to the highest concentration values. For completeness, the corresponding $N_{1,AV}$ range has also been reported for the experimental data by Dominijanni et al. (2013).

Fig. 4. Osmotic swelling pressure as a function of salt equilibrium concentration with best-fitting theoretical curve.

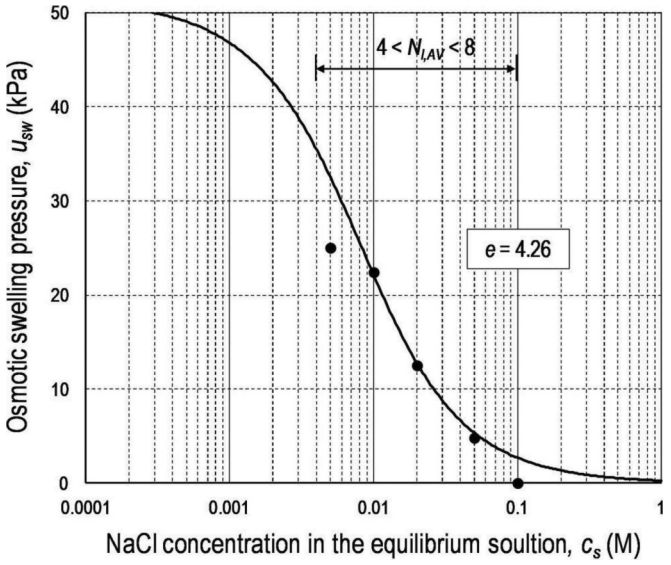

Fig. 5. Chemico-osmotic efficiency coefficient as a function of average salt concentration at top boundary of bentonite specimen with best-fitting theoretical curve (data from Dominijanni et al. 2013 and Shackelford et al. 2016).

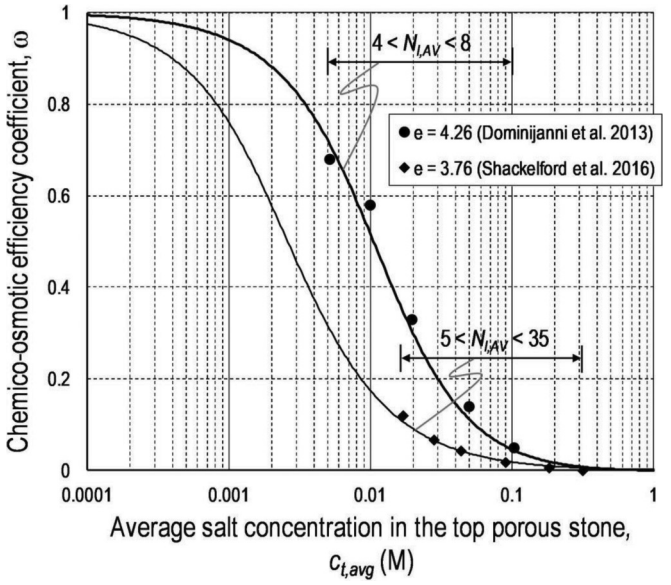

In general, the role played by the average number of lamellae per tactoid, in terms of osmotic swelling pressure and osmotic efficiency, decreases as the salt concentration of the external solution, c_s, increases and the osmotic efficiency approaches zero ($\omega \rightarrow 0$). However, other factors also may contribute to the differences in the diffusive behaviour of the two bentonites represented in Fig. 5, such as different void ratio, differences in the original (natural) salt content of the bentonite samples, and differences in how the specimens were prepared for testing.

Another significant validation of the proposed theoretical approach, in terms of osmotic efficiency, is given by the experimental data obtained from the aforementioned studies and plotted in Fig. 6. In this case, the theoretical linear relation from eq. (33) is in very good agreement with a large amount of experimental results. This excellent result can be considered another indication of the ability of the proposed theoretical framework to properly simulate the behaviour of bentonite systems in terms of osmotic efficiency.

Fig. 6. Restrictive tortuosity factor versus chemico-osmotic efficiency coefficient with the theoretical linear relation given by eq. (33).

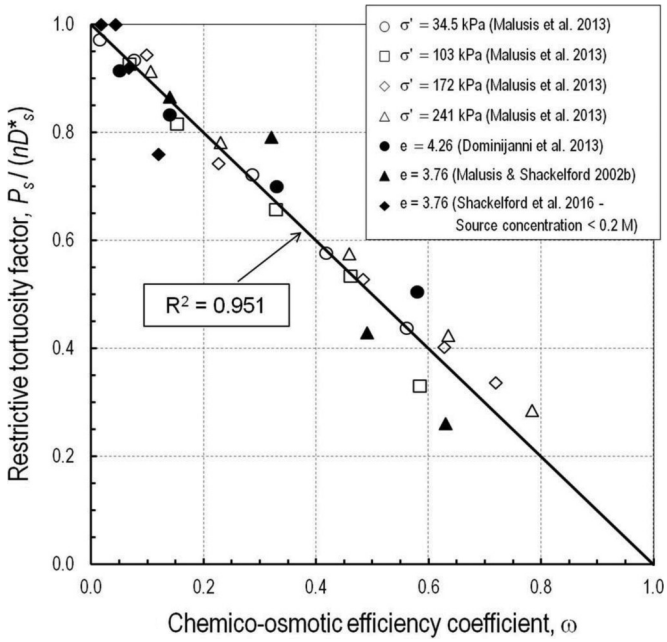

To extend the assessment of bentonite performance to a range of higher salt concentrations ($200 < c_s < 5000$ mmol·L^{-1}) and lower void ratios ($0 < e < 2$), a second series of results from different experimental studies that provide for more significant variation in bentonite fabric has been considered (see Tables 3 and 4) and, via the interpretation of hydraulic conductivity, oedometer, and swelling tests, the previously defined fabric parameters ($N_{1,AV}$, S_{eff}, and $\bar{c}_{sk,0}$) have been assessed. In the case of the high ion concentrations, the fabric of the bentonites undergoes major changes due to flocculation, particularly under low confining stress (i.e., high void ratio), resulting in a significant increase in the average number of platelets per tactoid and a corresponding decrease in the effective specific surface and solid skeleton effective electric charge concentration (Table 5). In contrast, at very low ion concentrations but under very high confining stress, the distance between the bentonite platelets decreases, resulting in the prevalence of attractive forces (van der Waals) relative to the repulsive electrochemical forces due to the negative charges on the platelet surface, with a consequent increase in the average number of lamellae per tactoid.

A comparison of this second series of experimental results with the theoretical predictions was conducted with the following considerations:

- Referring to the hydraulic conductivity tests on different bentonites and permeant solutions, an assessment of the effective specific surface, S_{eff}, has been performed using eq. (29) (Kozeny 1927; Carman 1956; Dominijanni et al. 2013), neglecting, as a first approximation, the electroviscosity coefficient, μ_{ev}, and referring to a steric tortuosity factor, τ_m, in the range from 0.2 to 0.3.
- An evaluation of the average number of platelets per tactoid, $N_{1,AV}$, and $\bar{c}_{sk,0}$ via eqs. (2*a*), (2*b*), and (13), respectively, and the assessment of the theoretical results in terms of osmotic swelling pressure, u_{sw}, by eq. (15) (Dominijanni et al. 2013) were performed. Comparisons of the obtained theoretical osmotic

Table 3. Intrinsic parameters of considered bentonites.

	Dominijanni et al. (2013), Puma et al. (2015), and Boffa (2016)	Malusis and Shackelford (2002*a*, 2002*b*)	Seiphoori (2014) and Manca (2015)	Mazzieri and Di Emidio (2011) and Mazzieri et al. (2013)	Di Emidio (2010)
Liquid limit, LL (%)	525	478	420	530	650
Plasticity index, PI (%)	—	439	355	480	600
Specific gravity, G_s	2.65	2.43	2.74	2.65	2.66
Principal minerals (%):					
Montmorillonite	98	71	85	90	95
Mixed-layer illite–smectite	—	7	—	—	—
Quartz	—	15	4	—	—
Other	—	7	11	—	—
Cation exchange capacity, CEC (meq·(100 g)$^{-1}$)	105	47.7	74.0	94.5	44.5
Stern coefficient, f_{Stern}	0.80, 0.90	0.90	0.70	0.85	0.80

Table 4. Range of state, fabric, and performance parameters of bentonites in contact with deionized water and NaCl, KCl, and $CaCl_2$ solutions.

	Dominijanni et al. (2013), Puma et al. (2015), and Boffa (2016)	Malusis and Shackelford (2002*a*, 2002*b*)	Seiphoori (2014)	Manca (2015)	Mazzieri Di Emidio (2011) and Mazzieri et al. (2013)	Di Emidio (2010)
Hydraulic conductivity, k (m/s)	6.00×10^{-12}	1.63×10^{-11}	1.0×10^{-14}	1.6×10^{-11}	6.5×10^{-11}	6.42×10^{-12}
	1.20×10^{-10}	—	1.0×10^{-13}	2.2×10^{-8}	—	—
Steric tortuosity factor, τ_m	0.30	0.14	0.20	0.30	0.35	0.35
	0.36	—	—	0.50	—	—
Total void ratio, e	0.60	3.76	0.53	2.15	5.13	2.55
	4.50	—	1.20	5.40	—	—
Micro-void ratio, e_m	0.10	2.56	0.05	1.23	3.6	1.13
	2.99	—	0.38	4.35	—	—
Effective diffusion coefficient, D_s^* (m^2·s^{-1})	5.0×10^{-10}	2.7×10^{-10}	—	—	—	—
Osmotic efficiency, ω	0.00	0.35	—	—	—	—
	0.68	—	—	—	—	—
Effective specific surface, S_{eff} (m^2·g^{-1})	24.14	164.40	36.18	6.09	159.65	129.94
	216.71	—	92.15	121.81	—	—
Average number of platelets per tactoid, $N_{1,AV}$	3.5	3.6	5.7	4.3	5.0	6.2
	31.5	—	14.5	85.9	—	—
Solid skeleton effective electric charge concentration, $\bar{c}_{sk,0}$ (mol·L^{-1})	0.008	0.046	0.035	0.003	0.100	0.041
	0.076	—	0.089	0.059	—	—

Table 5. Ranges of variation in monovalent ion equivalent concentrations that influence main performance parameters of bentonites at medium-to-high void ratios.

Main performance parameters of bentonite barriers	Range of monovalent ion concentration, c_s (mmol·L^{-1})	Notes
Osmotic efficiency, ω	0–100	No fabric variation For c_s higher than 100 mmol·L^{-1}, $\omega = 0$
Osmotic swelling pressure, u_{sw}	0–200	Small fabric variation For c_s around 200 mmol·L^{-1}, $u_{sw} = 0$
Hydraulic conductivity, k	200–5000	Significant fabric variation and significant k increments
Steric tortuosity factor, τ_m	200–5000	Significant fabric variation and significant τ_m increments

swelling pressure with the experimental swelling test results for the same bentonite samples are shown in Fig. 7.

- An additional assessment of the reliability of the proposed theoretical model, with reference to eq. (15), is shown in Fig. 8, where swelling and oedometer test results on samples permeated or hydrated with deionized water and with low concentration solutions ($c_s \leq 10$ mmol·L^{-1}) are shown together with the theoretical trend in terms of osmotic swelling pressure versus microvoid ratio.
- The good correlations obtained from comparing the theoretical model with experimental results in terms of osmotic efficiency, hydraulic conductivity and osmotic swelling pressures has provided the motivation to attempt to generalize the proposed framework as described subsequently.

Fabric parameters and related surface

As described previously, and considering the fundamental aspects concerning the complex chemicohydromechanical behaviour of bentonites, with particular reference to the use of bentonites as barriers for subsoil pollutant control, the fundamental role played by the fabric or structure of the solid skeleton once chemicohydromechanical equilibrium has been achieved is immediately apparent (Shackelford et al. 2000; Guyonnet et al. 2005; Bourg et al. 2006).

Fig. 7. Experimental versus theoretical osmotic swelling pressure using the fabric parameters obtained from hydraulic conductivity tests.

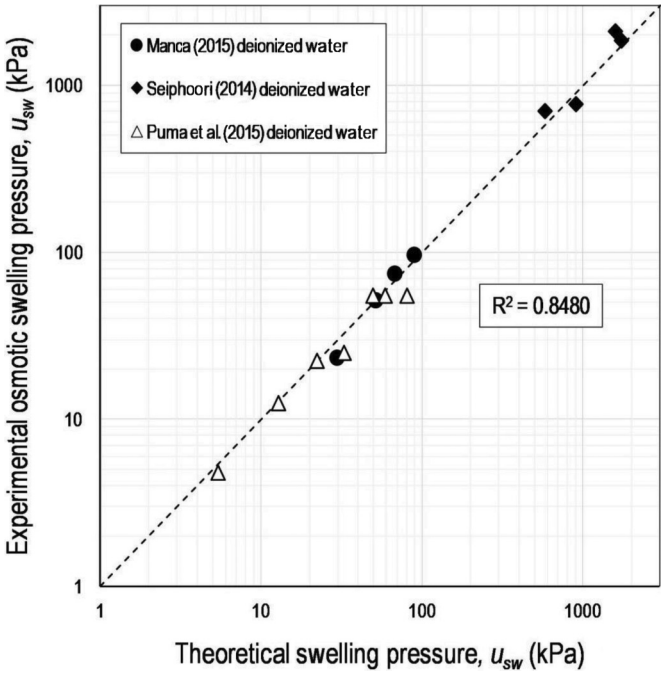

Fig. 8. Osmotic swelling pressure versus microvoid ratio for samples tested with deionized water and solutions with a monovalent ion equivalent concentration $c_s \leq 10$ mmol·L^{-1}.

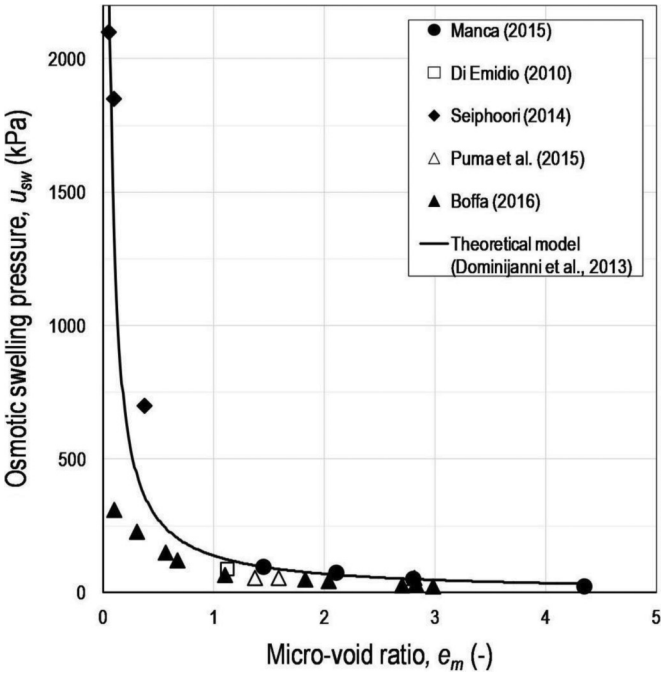

In terms of the conceptual schemes and possible evolution of the bentonite fabric under the actions of the previously described mechanical stress–strain and (or) electrolyte solution concentration, a series of fabric parameters (i.e., $N_{1,AV}$, S_{eff}, $\bar{c}_{sk,0}$), within which the most fundamental, direct, and clear one is the average number of platelets per tactoid, $N_{1,AV}$, can be introduced. The $N_{1,AV}$ fabric parameter plays a leading role in the second part of the proposed theoretical approach, in which an attempt is made to link the average number of platelets per tactoid, $N_{1,AV}$, to the two other parameters that define the external electrochemical and mechanical actions, i.e., the electrolyte concentration, c_s, and the microvoid ratio, e_m. The latter fabric parameter can be defined through the total void ratio, e, which is easy to determine via currently available laboratory tests, and the nano or interlayer void ratio, e_n, which can be evaluated, as a function of $N_{1,AV}$, from eq. (3), once b_n and d_{Stern} have been estimated with reference to their very limited ranges of variation, as defined previously.

Table 6. Some intrinsic, state. and fabric parameters for mechanical and chemicophysical models.

Field	Action	Intrinsic parameters	State and fabric parameters
Mechanical	Shear stress, τ	ρ_{sk}, φ_{cv}	e, p', ψ
Chemical	Ion concentration, c_s	S, σ, CEC, f_{Stern}	$N_{1,AV}$, S_{eff}, $\bar{c}_{sk,0}$

Note: φ_{cv}, friction angle at critical state; p', isotropic effective stress component; ψ, dilatancy angle; CEC, cation exchange capacity.

Average number of lamellae per tactoid

As already shown, $N_{1,AV}$ is directly linked to the effective specific surface, S_{eff}, and the solid skeleton effective electric charge concentration, $\bar{c}_{sk,0}$, through eqs. (2*a*) and (13). In particular, the effective specific surface, S_{eff}, is inversely proportional to the average number of platelets per tactoid, $N_{1,AV}$, through the intrinsic parameter, S (= 760 m^2·g^{-1}), i.e., the total specific surface of the single platelet. Moreover, the solid skeleton effective electric charge concentration, $\bar{c}_{sk,0}$, is also inversely proportional to $N_{1,AV}$ through four intrinsic parameters, i.e., the Faraday constant (F = 9.6485 × 10^4 C·mol^{-1}), the surface density of electric charge (σ = 0.114 C·m^{-2}), the density of the solid phase (ρ_{sk} = 2.75 g·m^{-3}), and the fraction of electric charge compensated by the cations specifically adsorbed in the Stern layer, f_{Stern}, which falls within a limited range ($0.70 < f_{Stern} < 0.95$). Therefore, the intrinsic parameter f_{Stern} could conveniently be used as a secondary fitting value to interpret a specific type of test conducted to investigate, e.g., the existence of still unproven or not precisely quantified flows, such as the hypothesized ionic diffusive surface flow (surface diffusion) within very dense bentonites and (or) the amount of cation exchange or sorption capacity during transient flow conditions (e.g., Glaus et al. 2007; Shackelford and Moore 2013).

Fabric boundary surface (FBS)

As noted previously, the proposed fabric parameters are primarily influenced by the concentrations of ions, c_s, in the pore solution and by the void ratio, which is in turn related to the effective isotropic component of the stress history of the bentonite. Once the family of fabric parameters that describe and quantify the lamellae arrangement at the nano- and microscales has been defined, a parallel development can be formulated with some aspects in common with the well-known elastoplastic work-hardening models of traditional soil mechanics (e.g., the Cam Clay model) for describing the mechanical behaviour of particulate media on the basis of a series of intrinsic and state parameters, as reported in Table 6.

As shown in detail in Dominijanni and Manassero (2012*a*, 2012*b*), among others, the framework that includes the previously defined intrinsic, state, and fabric parameters is capable of linking, through the Donnan, Navier–Stokes, and Nernst–Planck equations, the coupled transport phenomena for water and ions by imposing the general thermodynamic equilibrium between the bulk electrolyte solutions and the internal micropore solution at the macroscopic scale level. In addition, some specific aspects of mechanical behaviour can be modelled and coupled to the pore fluid transport by taking into account different types of intergranular actions, apart from the solid contact stress and the bulk pore pressure (Terzaghi 1943), such as electromagnetic at-

Fig. 9. Average number of platelets per tactoid, $N_{l,AV}$, versus micro void ratio, e_m, based on values from the interpretation of hydraulic conductivity, osmotic and swelling tests (fitting parameters: $N_{l,AV0}$ = 4.79, α = 0.91, β = 42.45; coefficient of determination, R^2 = 0.89).

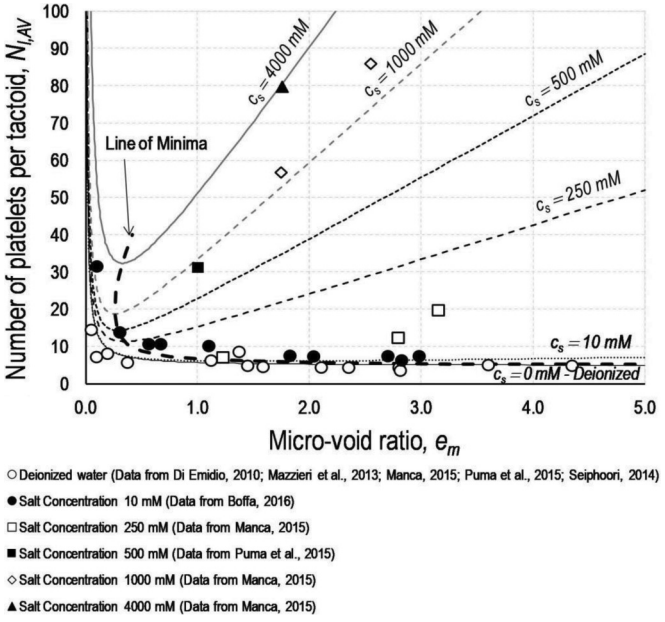

Fig. 10. Enlargement of Fig. 9 for the range $0 < N_{l,AV} < 20$.

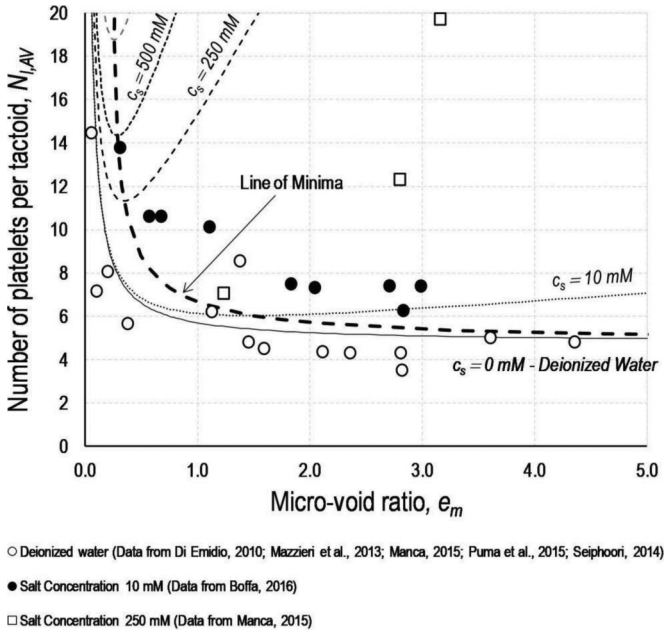

traction–repulsion and osmotic swelling–suction forces (Mitchell and Soga 2005).

In principle, and similar to the evolution of the basic Cam Clay model developed by Alonso et al. (1990) via the Universitat Politècnica de Catalunya (UPC) model for unsaturated soil, the intrinsic, state, and fabric parameters listed in Table 6 and the related framework can be extended to include the mechanical behaviour that is related to the fabric of the active fine-grained soils under fully saturated conditions, including not only actions such as the stress history and related void ratio, but also the ion species and concentration changes in the pore fluids. In the following description, the developed framework is applied to interpret the entire dataset from the aforementioned second series of experimental results taken from the literature and from the author's own laboratory tests, to illustrate the physical–chemical mechanisms that determine the observed macroscale behaviour of active clays.

Finally, the basic fabric parameter, $N_{l,AV}$, has been assessed with reference to bentonite samples, which were in contact with both deionized water and chemical solutions including those at high concentrations. This parameter, which provides a satisfactory prediction of the chemico-osmotic, hydraulic, and swelling–shrinking behaviour of bentonites, as illustrated previously, is directly linked to the other two fabric parameters, i.e., S_{eff} and $\bar{c}_{sk,0}$.

The resulting $N_{l,AV}$ values, each of which is associated with a specified electrolyte concentration, c_s, are plotted versus the microvoid ratio, e_m, in Figs. 9 and 10, with Fig. 10 simply representing the enlargement of the vertical axis close to the origin of Fig. 9.

To relate $N_{l,AV}$ to e_m and c_s, the following phenomenological equation, the trend of which has already been shown in Figs. 3*d*, 3*e*, and 3*f*, is proposed:

$$N_{l,AV} = N_{l,AV0} + \frac{\alpha}{e_m}\left(\frac{c_s}{c_0} + 1\right) + \beta e_m\left[1 - \exp\left(-\frac{c_s}{c_0}\right)\right] \quad (35)$$

where c_0 represents the reference concentration (= 1 mol·L^{-1}), $N_{l,AV0}$ is the ideal average minimum number of lamellae per tactoid when $c_s = 0$ and $e_m \to \infty$, α (= $e_m \cdot (N_{l,AV} - N_{l,AV0})$) is a coefficient relating $N_{l,AV}$ and e_m when $c_s = 0$, and β is a constriction coefficient that takes into account the limitation in movement of lamellae at medium-to-high void ratios due to mechanical constraints. The parameters $N_{l,AV0}$ and β both depend on the bentonite type, type of pre-treatments (e.g., removal of soluble salts, consolidation), hydration, and chemical exposure sequence.

The microvoid ratio, e_m, in eq. (35) can be derived from the total void ratio through the following equation:

$$e_m = \frac{eN_{l,AV} - S\rho_{sk}b_n(N_{l,AV} + d_d - 1)}{N_{l,AV}} \quad (36)$$

By substituting eq. (36) into eq. (35), the number of lamellae per tactoid is related to the total void ratio and the salt concentration through a cubic equation, which can be solved analytically or numerically for given values of the parameters $N_{l,AV0}$, α, β, S, ρ_{sk}, b_n, and d_d. The available experimental data were regressed by imposing $N_{l,AV0}$ = 4.79, α = 0.91, and β = 42.45 (coefficient of determination, R^2 = 0.89).

Equation (35) can be considered as an operative and simplified version of the formal theoretical equation reported in Figs. 3*a*, 3*b*, and 3*c* for medium-to-high void ratios. As shown in Figs. 3*d*, 3*e*, and 3*f*, which reflect eq. (35), a good agreement between the two surfaces is apparent, particularly with respect to the ascending branch versus the increasing microvoid ratio. This good agreement can be considered as further validation of the interpretation of the experimental data by the proposed simplified model through a formal and rigorous theoretical approach for medium-to-high e_m values.

Using this latter FBS equation (eq. (35)) for the proposed simplified model, it is interesting to consider the regression results in terms of the average number of lamellae per tactoid as obtained from the interpretation of the aforementioned hydraulic conductivity and swelling tests belonging to the second series of experimental data. The average number of lamellae per tactoid plotted versus the microvoid ratio (i.e., the intertactoids void ratio) in particular shows an interesting but expected trend. In fact, for any given electrolyte concentration (apart from the unique case of deionized water), an initial decrease in $N_{l,AV}$ to a minimum value is followed by a continuous increasing trend with corresponding

increase in the microvoid ratio. More specifically, the ideal line, which represents the minimum loci of the aforementioned functions at the different ion concentrations, c_s, of the solutions in contact with the bentonite versus e_m, may represent a separation locus between flocculating and dispersive behaviour of the considered bentonites, in a similar way to the case of unsaturated soils where swelling and shrinking behaviours are dependent on the degree of saturation (or suction) versus the confining stress and related void ratio (Alonso et al. 1990).

Some 3D views of the proposed FBS in the domain defined by the number of lamellae per tactoid, $N_{l,AV}$; the microvoid ratio, e_m; and the electrolyte concentration, c_s; are reported in Fig. 11, together with the profiles defined by planar sections orthogonal to the primary axes.

Determination of FBS parameters

To determine the parameters of the FBS, i.e., $N_{l,AV0}$, α, and β, for a specific bentonite, an experimental procedure, which minimizes the number of required laboratory tests, can be performed as follows.

First, two swelling tests at two different values of the total void ratio, e, are required to measure the osmotic swelling pressure in equilibrium with deionized water (i.e., with a solution having a null salt concentration, $c_s = 0$) under constant volume conditions. Because, on the basis of eq. (15), the osmotic swelling pressure is a function of the microvoid ratio, e_m, and the number of lamellae per tactoid, $N_{l,AV}$, two values of $N_{l,AV}$ can be derived from the inversion of this relation, if assumptions on the values to be assigned to d_d (≈ 4) and f_{Stern} (≈ 0.85) are made. Once these two values of $N_{l,AV}$ have been obtained, the parameters $N_{l,AV0}$ and α can be calculated using the following equation:

$$\alpha = (N_{l,AV} - N_{l,AV0})e_m \tag{37}$$

which results from eq. (35) for $c_s = 0$.

Second, a single hydraulic conductivity test is needed using a permeant solution with a salt concentration, c_s, equal to the reference concentration, c_0 (= 1 mol·L^{-1}), to determine the value of $N_{l,AV}$ from the inversion of eq. (29) by neglecting, as a first approximation, the electroviscosity and assigning a value for the matrix tortuosity, τ_m. The parameter β can be obtained from this value of $N_{l,AV}$ through the following equation:

$$\beta = \left[\frac{\exp(1)}{\exp(1) - 1}\right]\left[\frac{e_m(N_{l,AV} - N_{l,AV0}) - 2\alpha}{e_m^2}\right] \tag{38}$$

which is derived from eq. (35) for $c_s = c_0$.

If the tests for the aforementioned experimental procedure are not available, then the fabric boundary surface parameters can be estimated by implementing a best-fitting procedure on a set of data defined in the space of the variables $N_{l,AV}$, e_m, and c_s, which are obtained from the interpretation of other laboratory test results. This last calibration method has been adopted for the estimation of the fabric boundary surface parameters that were described in the previous section.

Validation of theoretical model

After establishing the last comprehensive version of the theoretical model introduced within the previous section, an additional validation was performed using a third series of experimental results reported in the literature and including direct and indirect measurements or assessments of the number of lamellae per tactoid versus microvoid ratio and salt concentration in the external solution in equilibrium with the pore solution of the tested bentonites.

More specifically, in this last series of tests, particular attention has been given to the reliability of the model for the range of reduced microvoid ratio ($0 < e_m < 1$) consistent with the typical bentonite used in confinement systems for HLRW. Moreover, the influence of the interaction with the geosynthetic fibres present in GCLs has also been considered, due to the increasing use of these products in modern landfill lining systems.

Experimental tests and results

Prior to presenting a comparison of the experimental results with theoretical predictions, a summary of the primary aspects of direct and indirect tests and experimental techniques that have been used to determine the $N_{l,AV}$ values of the considered bentonites at different void ratios and salt solution concentrations is worthwhile. This review also will illustrate the uncertainties and complexities associated with the estimation procedures for the assessment of the average number of lamellae per tactoid of active clays and the expected reliability and precision of the different techniques.

Direct methods

Several experimental approaches, such as electron microscopies, spectroscopic analyses, and diffraction techniques, have been used to provide a direct assessment of the pore structure in compacted unsaturated and saturated bentonites, as the ratio of interlayer or intratactoid to noninterlayer or intertactoid water represents a key parameter governing water and solute transport.

Imaging techniques have been used extensively to observe bentonite microstructure (Laird et al. 1989; Tessier 1990). Viola et al. (2005) described the use of two innovative methods derived from traditional scanning electron microscopy (SEM), viz., field emission SEM (FESEM), which includes a field emission electron emitter that is brighter and, therefore, yields higher resolution than thermal emitters used in traditional SEM; and environmental SEM (ESEM), which offers the ability to observe porous materials under different hydration states without specific requirements for sample preparation.

FESEM micrographs can reach a magnification of 10 000×, which allows observation of the spatial arrangement of tactoids. However, FESEM is limited by the sample preparation procedure, which requires a freezing process followed by ice transformation to vapour phase to obtain a dried sample with a preserved microstructure. In contrast, ESEM analysis can be conducted directly on undisturbed hydrated samples in the microscope sample chamber. With this promising technique, the evolution of mesopores in sand bentonite mixtures can be observed during a dehydration process (Viola et al. 2005).

Transmission electron microscopy (TEM) is a high-resolution imaging technique that allows observation of the montmorillonite lamellae structure in compacted unsaturated and saturated bentonites over a wide range of magnifications (Matusewicz et al. 2013). TEM provides an observation of various microstructural features, such as nanometre-sized pores and the arrangement of dense tactoids of montmorillonite layers.

A limitation of the aforementioned imaging techniques is that the micrographs show only an extremely small portion of bentonite volume, at a scale ranging from a few micrometres to less than a nanometre, thus having a limited representativeness (Guyonnet et al. 2005). Furthermore, the methods do not provide a quantification of the interlayer and noninterlayer pore volumes, or the average distance between the tactoids and between the lamellae inside the tactoids.

A common approach for the investigation of the intratactoid pore space of montmorillonite is to apply XRD techniques to monitor intratactoid expansion (Norrish 1954). The XRD technique is based on the interaction of X-rays with the atomic plane in the mineral crystalline structure. Reflections defining atomic plane spacings, primarily the basal spacing, d_{001}, are used in combination

Fig. 11. Fabric boundary surface (FBS): (*a*, *b*, *c*) 3D image; (*d*, *e*, *f*) planar section traces.

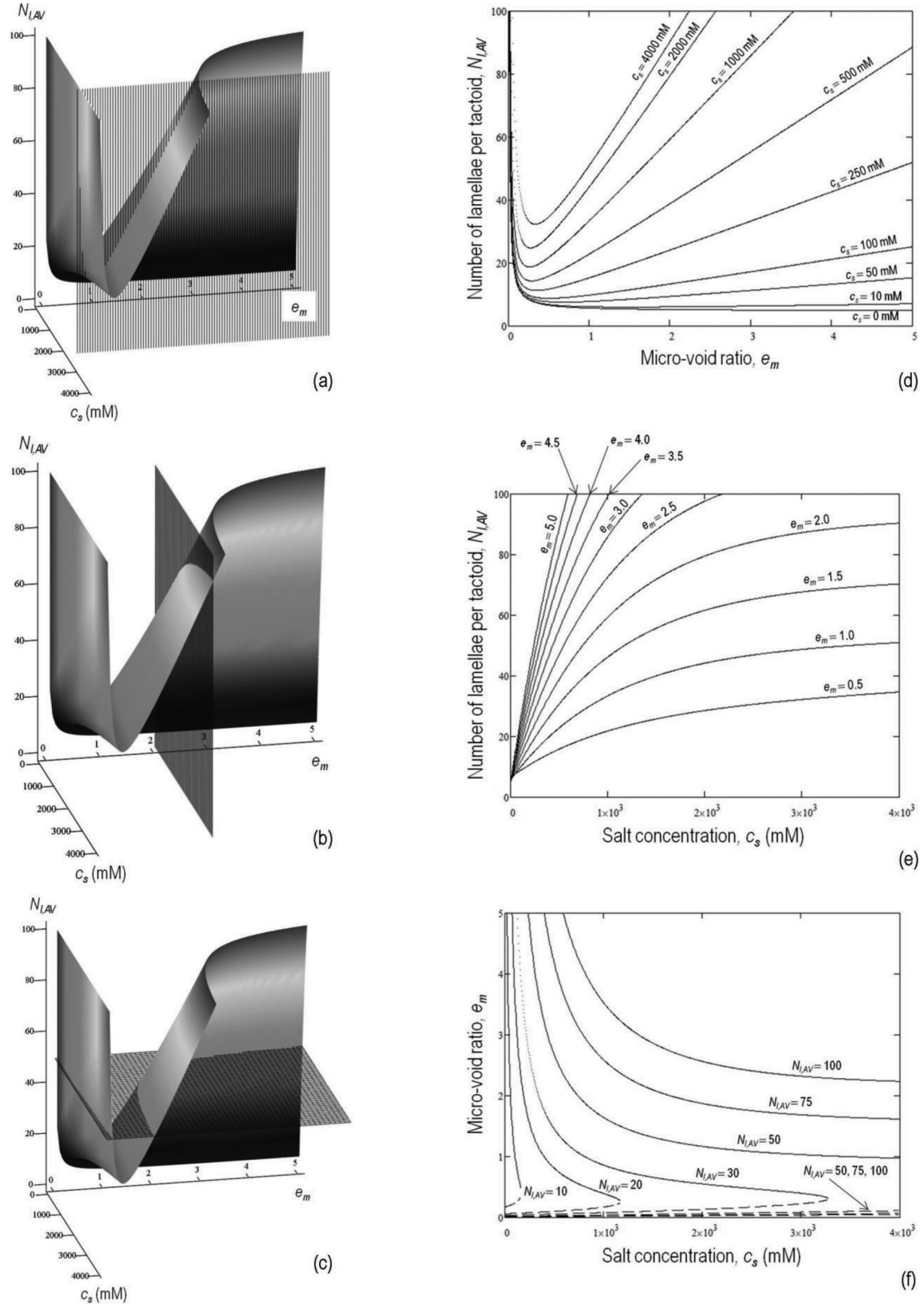

with their integrated areas for mineral identification (Likos et al. 2010). However, the information provided by XRD analyses can be complicated by interstratification, because the combined effects of various basal spacings are not easily distinguished from those due to particle size, morphology, and orientation (Laird et al. 1989).

Muurinen et al. (2013) adopted SAXS to study the changes in intratactoid distances for bentonite samples. From these measurements, peak profile modelling was used to estimate the respective contributions of various mixed-layer structures to the observed peaks.

Although the diffraction techniques provide insight into the alignment existing in stacked layers, these techniques do not directly detect disordered complex intertactoid geometries. In contrast, low field ^{1}H NMR is a reliable method for intertactoid and intratactoid volume characterization and quantification (Manalo et al. 2003; Todoruk et al. 2003; Mitchell et al. 2008). The principle of the ^{1}H NMR relaxometry is related to changes in the magnetization owing to spin relaxation of protons back to equilibrium after excitation with an external static magnetic field. Spin relaxation is faster in the vicinity of solid surfaces, which is due to restriction of water mobility and interactions of protons with magnetic impurities along the pore wall, such as Mn^{2+} and Fe^{3+}. As compacted saturated bentonites have a heterogeneous structure, pores are not isolated and NMR relaxation data are sums of exponentially decaying components, reflecting local surface-to-volume ratios. Experimental results may be transformed into pore-size distributions by the so-called inversion of the decay data (Borgia et al. 1998).

NMR has previously been used successfully to determine the distribution of pore water in water-saturated bentonites (e.g., Ohkubo et al. 2008, 2016; Montavon et al. 2009; Muurinen et al. 2013). Through an interpretation of the differences in observed proton mobilities, Montavon et al. (2009) were able to distinguish between three different populations, i.e., structural OH, external surface water, and internal surface water. The problem of rapid exchange between external surface water and bulk water in water-saturated clays was solved by freezing samples to –25 °C. At this temperature, the bulk water was frozen and, thus, distinguishable from the surface water that was in a semi-liquid state.

To overcome the aforementioned lack of a clear differentiation of these types of water, Ohkubo et al. (2008) assumed that the relaxation time corresponding to a three-hydrated layer space can be used to distinguish intratactoid and intertactoid water, whereas Ohkubo et al. (2016) adopted both methodologies described above (i.e., the selective freezing of the bulk water and the assumption of the relaxation time of a three-hydrated layer space as the threshold between the bulk and surface water) to investigate the salt concentration effect of a NaCl solution on the pore-size distribution of compacted montmorillonite. By fitting discrete exponentials to the decay curves obtained from NMR measurements, Muurinen et al. (2013) found that the observed relaxation was composed of two major relaxation processes, and that assuming a third relaxation process produced a marginal effect. On the basis of these results, Muurinen et al. (2013) suggest the presence of only two water phases in water-saturated smectitic clays, viz., interlayer and noninterlayer water.

Indirect methods

Several indirect methods may be adopted to evaluate the microstructure of water-saturated bentonite and montmorillonite (i.e., how water is distributed between different pores in the clay fabric). In contrast to the direct methods, these approaches require defining a structural model for the clayey soil as well as the relationship linking the intrinsic, state, and fabric parameters to the phenomenological parameters, which are measured by means of laboratory tests.

In light of the aforementioned theoretical framework, the osmotic efficiency, ω, in eq. (30) is a function of the basic fabric parameter, $N_{1,AV}$, through the solid skeleton effective electric charge concentration, $\bar{c}_{sk,0}$. Thus, measurements of chemico-osmotic efficiency could be used to estimate the average number of lamellae per tactoid and to predict the pore-water distribution on the basis of eq. (36). However, the chemico-osmotic efficiency is negligible at high electrolyte concentrations ($c_s > 100$ mmol·L^{-1}), such that detecting the soil fabric changes in response to variations in the ionic strength of the equilibrium solution is not possible (e.g., Shackelford et al. 2016 found $0 < \omega < 0.02$ for $c_s \geq 100$ mmol·L^{-1}).

A similar discussion pertains to swelling pressure tests, given that the bentonite chemico-osmotic swelling pressure decreases to negligible values at high electrolyte concentrations ($c_s >$ 200 mmol·L^{-1}). In addition, a potentially significant uncertainty is associated with laboratory tests performed to measure swell pressure. For example, some studies conducted to measure the swell pressure of active clays have reported unexpectedly high values that are inconsistent with the specified boundary conditions (see e.g., Karnland et al. 2005). The observed disagreement between the measured and predicted pressures can be attributed to the testing procedures, due to the lack of recognition associated with the complete dissipation of the suction component with hydration of an initially unsaturated specimen.

Unlike the aforementioned phenomenological parameters, the hydraulic conductivity of smectitic clays undergoes significant changes as a result of different arrangements of the unit layers or lamellae in the soil fabric, which in turn influence the microvoid space accessible for advective transport and the effective specific surface. Therefore, hydraulic conductivity (permeability) tests represent an effective tool for investigating flocculation within a wide range of soil porosities and salt concentrations of the permeant solution. Additionally, according to eq. (29) and neglecting the electroviscous effect, the interpretation of hydraulic conductivity tests is independent of the value for the Stern fraction, f_{Stern}.

Other indirect experimental procedures have been found to be useful for the examination of the microstructure of active clays. For instance, the anion exclusion effect has recently been studied by means of different techniques. Van Loon et al. (2007) recognize that the diffusive behaviour of anions is a complex function of the electrochemical interactions between the solutes and the porous medium. Indeed, in the case of negatively charged surfaces, anions are expelled from the DDL leading to a "negative adsorption" (Bolt and de Haan 1982; Pusch et al. 1990), the extension of which depends on the composition of the equilibrium solution and the degree of compaction. Van Loon et al. (2007) were able to estimate accessible porosities for chloride ions by interpreting the results of through-diffusion and out-diffusion tests performed on a Volclay KWK bentonite using the radionuclide $^{36}Cl^-$ as a nonsorbing tracer, and also by determining the concentration profile of stable Cl^-. In this latter case, upon completion of the out-diffusion test, the bentonite specimen was sliced in 1 mm thick pieces, which were then dispersed in deionized water. Further details about these experimental procedures can be found in Molera et al. (2003), García-Gutiérrez et al. (2004), Muurinen et al. (2004, 2007, 2013), Birgersson and Karnland (2009), and Tournassat and Appelo (2011). Under the hypothesis of complete exclusion of anions from the intratactoid space and from the Stern layer, which together represent the nanovoid space, because anions are only partially repulsed from the larger pores of the inter-tactoid space, the ion partition coefficient, Γ_2, given by eq. (12), must be equal to the ratio of the anion accessible porosity, n^*, to the microvoid porosity, n_m. Thus, based on this observation, determining the value of the fabric parameter $N_{1,AV}$ and the relative amounts of the different pore types is possible.

Theoretical predictions and comparison

The aforementioned third series of experimental results was used to validate the robustness of the proposed theoretical model, avoiding any further calibration of the FBS defining parameters.

Initially, results obtained through NMR measurements were analysed (Muurinen et al. 2013; Matusewicz et al. 2013; Ohkubo et al. 2016). The intrinsic, state and fabric parameters of bentonites tested through this method are reported in Tables 7 and 8, respectively. This analysis of the soil microstructure can be considered as a direct method, strictly speaking, because no assumptions need to be made with respect to the electrochemical interactions that occur at the microscale or with reference to the arrangement of unit layers or lamellae. In fact, when the ratio of the intratactoid to the intertactoid pore space is known, eqs. (2)–(4) are sufficient to determine an average number of lamellae per tactoid.

In terms of high void ratios, Fig. 12 shows reasonably good agreement between the experimental data and the proposed fabric boundary surface. In contrast, this agreement becomes poorer with the increase in compaction degree.

The same conclusion is more effectively detailed in Fig. 13. In fact, the data related to the lowest void ratios have to be omitted from the regression to obtain a reasonably good coefficient of determination.

A possible explanation for this observation can be obtained by taking the physical significance of the NMR results into account, as there is a risk of underestimating the intertactoid porosity. In very high density samples, the difference between the average size of the intertactoid pores and the intratactoid pores is not sufficiently large to discern the two pore types with this method (Järvinen et al. 2016). Thus, further study is recommended to improve the reliability of NMR for fine-grained soils, with a focus on evaluating to what extent the behaviour of the water contained inside the conductive pores is affected by magnetic interactions with the solid phase.

Muurinen et al. (2013) also performed SAXS measurements on the same Na–bentonite tested by NMR, and based on the measured basal distances, they were able to compute the amounts of intratactoid water. Obviously, a similar computation requires the a priori definition of the internal specific surface (i.e., the fabric parameter $N_{l,AV}$), which was used by Muurinen et al. (2013) as a fitting parameter. Despite the uncertainty connected with this fitting approach, the interpretation of the data through the proposed fabric boundary surface can be considered satisfactory (Fig. 12).

In Fig. 14, experimental results obtained from indirect methods are compared versus theoretical predictions. For this purpose, hydraulic conductivity (Jo et al. 2004; Lee and Shackelford 2005; Katsumi et al. 2008; Shackelford et al. 2016; Ewy 2017) and anion exclusion tests (Muurinen et al. 1989, 2013; Van Loon et al. 2007) are considered. The intrinsic, state and fabric parameters of bentonites tested through indirect methods (i.e., hydraulic conductivity tests and anion exclusion tests) are reported in Tables 9–12.

Whereas data from Jo et al. (2004) and Ewy (2017) refer to a natural granular Na–bentonite and to shale samples, respectively, the other studies were based on permeability tests with deionized water on GCL specimens. Indeed, the hydraulic conductivity of GCLs can be affected by the needle-punching process. However, Puma et al. (2015) showed that the presence of needling across a GCL sample does not hinder swelling during hydration and does not influence the hydraulic conductivity of bentonites that are permeated by deionized water or dilute aqueous solutions. The agreement between the literature data and the previously defined fabric boundary surface is good, and the scatter indicated in Fig. 13 can be ascribed to the large variety of clay types considered in this study.

Table 7. Intrinsic parameters of bentonites whose microstructure was experimentally investigated through direct methods.

	Muurinen et al. (2013) and Matusewicz et al. (2013)	Ohkubo et al. (2016)
Specific gravity of solids, G_s	2.75	2.80
Total specific surface ($m^2 \cdot g^{-1}$)	610	760
Principal minerals (%)		
Montmorillonite	83.5	98.0
Mixed-layer illite–smectite	0.7	—
Quartz	2.8	—
Other	—	—
Cation exchange capacity, CEC ($meq \cdot (100\ g)^{-1}$)	84.0	—
Stern coefficient, f_{Stern}	0.85	0.85

Table 8. Range of state and fabric parameters of bentonites whose microstructure was experimentally investigated through direct methods.

	Muurinen et al. (2013)	Matusewicz et al. (2013)	Ohkubo et al. (2016)
Total void ratio, e	0.72	0.81	1.00
	2.93	3.37	2.50
Microvoid ratio, e_m	0.19	0.01	0.00
	1.89	3.20	1.39
Effective specific surface, S_{eff} ($m^2 \cdot g^{-1}$)	21.32	18.03	68.97
	73.58	74.48	86.07
Average number of platelets per tactoid, $N_{l,AV}$	8.3	8.2	8.8
	28.6	33.8	11.0
Solid skeleton effective electric charge concentration, $\bar{c}_{sk,0}$ ($mol \cdot L^{-1}$)	0.010	0.009	0.034
	0.036	0.036	0.043

Finally, an attempt was made to verify the possibility of adjusting the FBS parameters $N_{l,AV0}$, α, and β on a given set of tests results, related to the same clayey soil. In fact, all the elastoplastic constitutive laws adopted, for instance, in traditional soil mechanics (e.g., Cam Clay model) must be calibrated on a restricted dataset pertaining to a specific clay. Accordingly, the parameters defining the proposed hydrochemicomechanical coupled model should also be differentiated for each tested clay, and the values of the FBS parameters specified previously can be used just as a rough approximation of the actual behaviour.

The experimental results provided by Petrov and Rowe (1997) were chosen for this analysis. The authors conducted hydraulic conductivity tests on a needle-punched GCL, subjected to prehydration with distilled water (DW). The tests covered a wide range of effective confining stresses (from 3.4 to 114 kPa) and concentrations of the permeant NaCl solutions (from 0.01 to 2.0 $mol \cdot L^{-1}$), thus providing a sizeable range of data available for calibration. The intrinsic, state and fabric parameters of the GCL tested by Petrov and Rowe (1997) are reported in Tables 9 and 10, respectively. Incidentally, for this set of data, the interpretation via the same model (intrinsic) parameters adjusted for natural bentonites may be conceptually incorrect, because of the potential impact resulting from the presence of the needle-punched fibres, which is expected to cause higher values of hydraulic conductivity due to the formation of preferential flow pathways along the fibres of the needling treatment when the GCL is permeated with solutions having a high salt concentration (Puma et al. 2015).

In Fig. 15, the ordinary least-squares method has been applied for the data regression ($N_{l,AV0} = 1.56$, $\alpha = 8.82$, $\beta = 10.01$), and a high coefficient of determination has been obtained ($R^2 = 0.9384$) as shown in Fig. 16. These results highlight the reliability of the simplified equation of the FBS, and the ability to simulate the coupled chemicomechanical behaviour of active clays, once

Fig. 12. Comparison between FBS and experimental results taken from specialized literature (direct methods): (*a*) $N_{1,AV}$ versus e_m; (*b*) $N_{1,AV}$ versus c_s; (*c*) $N_{1,AV}$ versus c_s.

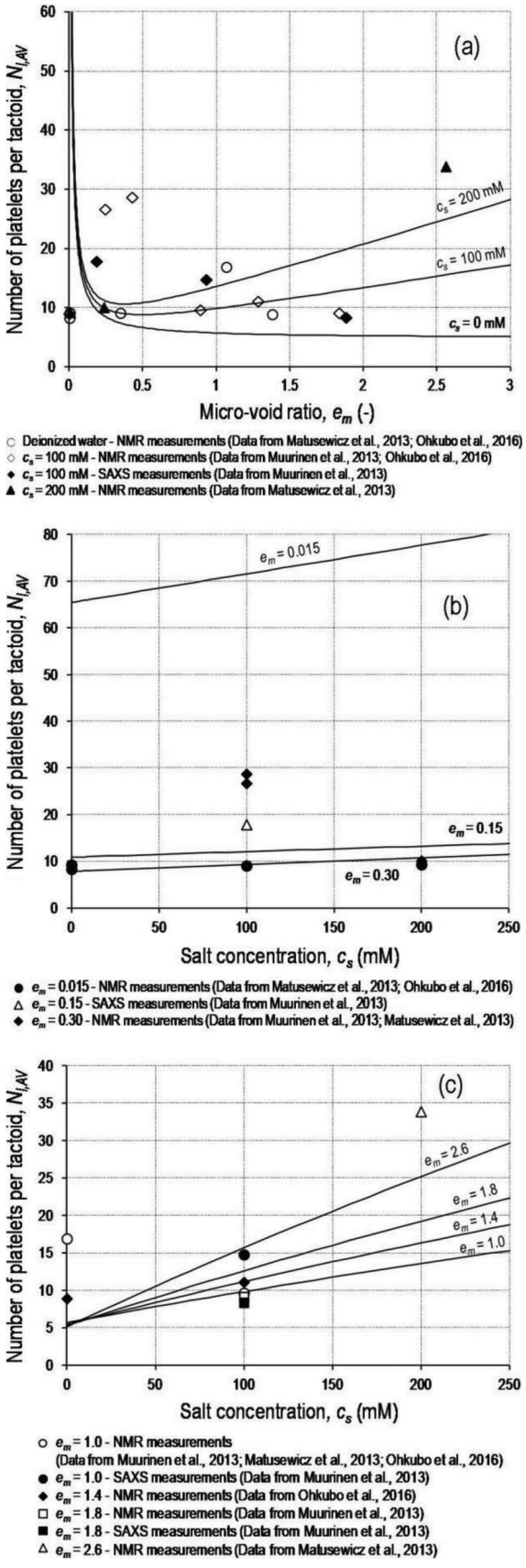

Fig. 13. Experimental versus theoretical average number of lamellae per tactoid $N_{1,AV}$, using literature data obtained through direct and indirect measurement methods (note: question-marked points have not been used to compute coefficient of determination).

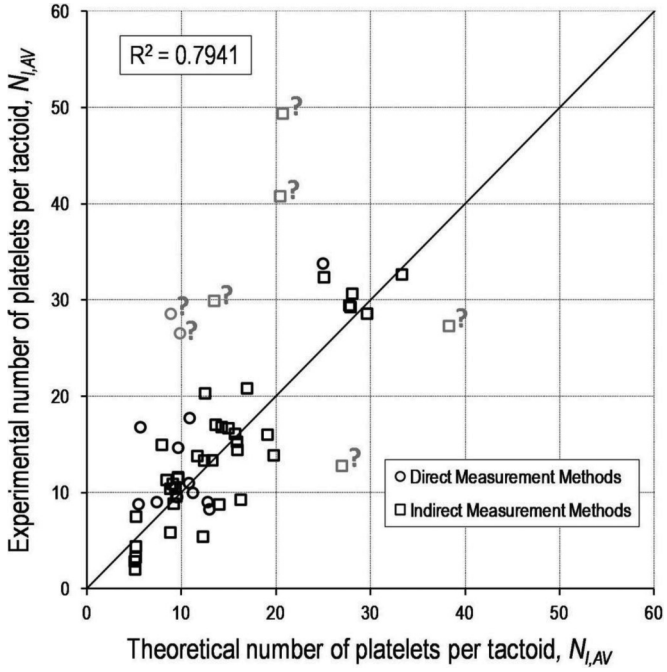

the model parameters have been properly assessed for the specific bentonite under consideration.

Critical issues concerning assessement of intrinsic parameters

Among the three main categories of input data, i.e., intrinsic, state, and fabric parameters, which have to be determined for an appropriate and reliable use of the proposed theoretical model, an important role is played by some basic intrinsic parameters and, in particular, by the cation exchange capacity, CEC, and the Stern fraction, f_{Stern}.

Under the assumptions of a perfectly dispersed microstructure and a complete ion exchange process during the experimental assessment of the cation exchange capacity of a given clay, as commonly hypothesized for standardized laboratory tests, the CEC and f_{Stern} can be related directly (together with the solid phase density, ρ_{sk}) to the two primary fabric parameters of the proposed model, i.e., the molar concentration of the solid skeleton effective electric charge, $\bar{c}_{sk,0}$, and the average number of lamellae per tactoid, $N_{1,AV}$, as follows (Dominijanni and Manassero 2012*b*):

$$\bar{c}_{sk,0} = \frac{1 - f_{Stern}}{N_{1,AV}} CEC \rho_{sk} \quad (39)$$

Moreover, the CEC can in turn be linked to other intrinsic parameters and a chemical constant, i.e., the surface density of electric charge, σ, the total specific surface of the single lamella, S, and the Faraday constant, F, through the following equation:

$$CEC = \sigma \frac{S}{F} \quad (40)$$

Although the determination of CEC alone is not sufficient to allow an evaluation of $\bar{c}_{sk,0}$ and (or) $N_{1,AV}$, CEC plays a fundamental role

Fig. 14. Comparison between FBS and experimental results taken from speciealized literature (indirect methods): (*a*) $N_{l,AV}$ versus e_m; (*b*) $N_{l,AV}$ versus c_s; (*c*) $N_{l,AV}$ versus c_s.

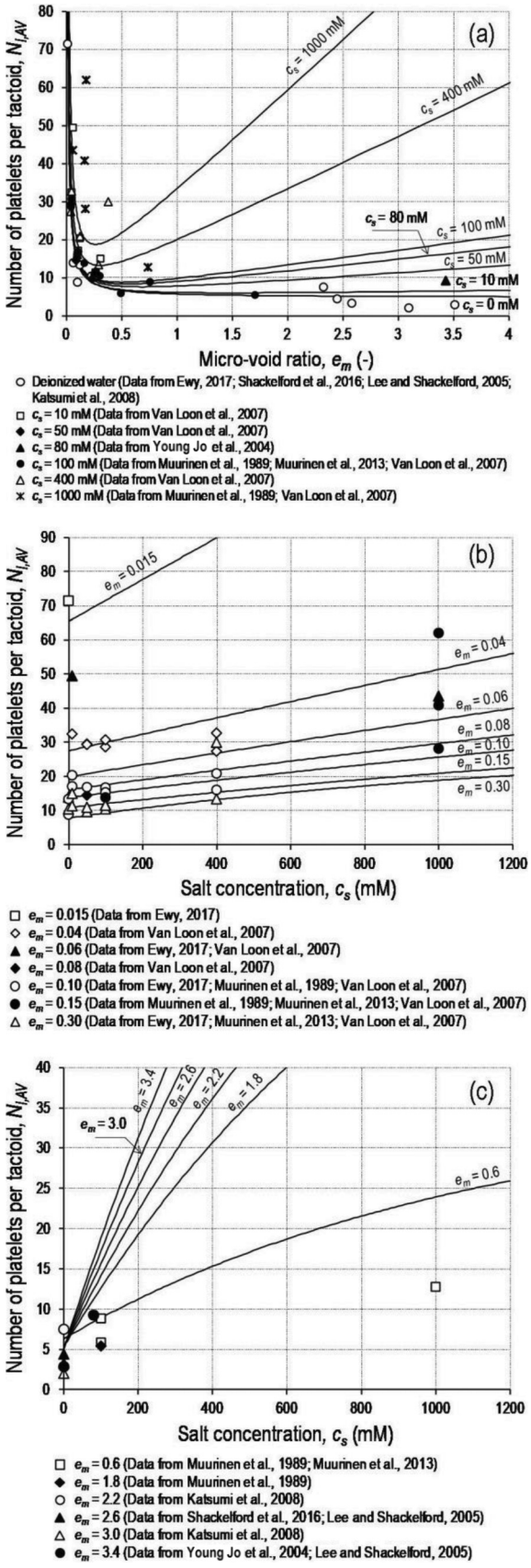

in relating the physical and chemical properties of bentonite, at the pore scale, to the macroscopic constitutive parameters. For this reason, a series of experimental tests has been conducted on the same bentonite clay used by Puma et al. (2015) to assess the reliability of the most commonly adopted CEC measurement methods, including the ammonium displacement method (ADM) and the methylene blue titration method (MBM), which are described subsequently.

Testing procedures

Exchange with ammonium acetate is a standard method for CEC determination of fine-grained inorganic soils (ASTM 2010) such as bentonite. This procedure was adopted to determine the "standard" CEC value. In brief, 10 g of bentonite solids was mixed with 40 mL of 1 mol·L^{-1} ammonium acetate in 250 mL polypropylene bottles and agitated for 5 min. After 24 h, the slurry was again agitated for 15 min and then transferred to a 96 mm diameter ceramic Buchner funnel lined with filter paper (>2.5 μm particle retention capacity) and placed on top of a filtering flask connected to a vacuum pump. The soil was then washed under low vacuum (<10 kPa) with four 30 mL additions of ammonium acetate. Three 40 mL additions of isopropanol were filtered through the soil under vacuum to remove the excess ammonium acetate and the filtrate was discarded. The subsequent step consisted in filtering four 50 mL additions of 1 mol·L^{-1} KCl through the bentonite layer. The filtrate was collected and transferred to a 250 mL volumetric flask filled to capacity with DW. The obtained final solution was analysed to establish the concentration of ammonium ions, NH_4^+.

The standard procedure was modified slightly by using different KCl concentrations (4.5, 0.1, 0.05, 0.025, 0.010, 0.0025, 0.001 mol·L^{-1}) and DW, to investigate the effect of changes in the bentonite structure on the CEC results. The modified procedure was identical to the standard procedure, except for the last phase in which each solution was filtered through the soil instead of 1 mol·L^{-1} KCl. The tests generally were duplicated.

The MBM is a rapid, qualitative procedure used by industry for routine quality control, which provides a measure of the accessible anionic sites in a condition of enhanced dispersion of the clay. The MBM test was carried out following the procedure outlined in EUBA (2002).

Test results

The CEC measurement results are listed in Table 13 and plotted in Fig. 17. The solid symbols in Fig. 17 represent the CEC values obtained from the measured amount of NH_4^+ released. The values obtained using DW are plotted at 0.1 mmol·L^{-1} KCl concentration. Considering the average of measurements for each extracting solution concentration, the maximum CEC measured with NH_4^+ is 84.5 meq·(100 g^{-1}) (0.1 mol·L^{-1} KCl solution), which is lower than the values obtained with the MBM tests (97 and 104 meq·(100 g^{-1})). Thus, for the sake of simplicity, the mean CEC value is plotted in Fig. 17.

The results suggest that the measured CEC depends on the aggregation state of the bentonite particles. In particular, the MBM test seems to provide an upper bound of the measured CEC due to the disperse state of the bentonite, which enhances the accessibility of exchange sites with respect to the particle aggregation that occurs with the standard test procedure (1 mol·L^{-1} KCl solution). Despite some scatter in the results, the average CEC versus KCl concentration tends to be practically constant for KCl > 0.1 mol·L^{-1}, suggesting a similar aggregation condition of the bentonite particles. As the KCl concentration decreased (<0.1 mol·L^{-1}), the CEC calculated from released NH_4^+ also decreased. However, the amount of potassium ions, K^+, available for exchange also decreased. The maximum theoretically measurable CEC, based on the available K^+, is also shown in Fig. 17. The measured CEC for low (<20 mmol·L^{-1}) to practically zero (DW) KCl concentrations ranged from 13.9 to 23.9 meq·(100 g^{-1}), which is higher than the theoret-

Table 9. Intrinsic parameters of bentonites whose microstructure was experimentally investigated through indirect methods (hydraulic conductivity tests).

		Lee and Shackelford (2005)					
	Jo et al. (2004)	LQB	HQB	Katsumi et al. (2008)	Shackelford et al. (2016)	Ewy (2017)	Petrov and Rowe (1997)
Liquid limit, LL (%)	504	430	589	619.5	478	—	—
Plasticity index, PI (%)	465	393	548	568.5	439	—	—
Specific gravity of solids, G_s	2.65	2.74	2.78	2.839	2.68	2.70	2.61
Total specific surface ($m^2 \cdot g^{-1}$)	620	540	790	880	650	250	750
Principal minerals (%)							
Montmorillonite	81.0	77.2	86.0	—	71.0	—	91.0
Mixed-layer illite–smectite	—	—	—	—	7.0	46.0	—
Quartz	—	3.4	3.5	—	15.0	20.0	5.0
Other	—	—	—	—	7.0	—	—
Cation exchange capacity, CEC (meq·(100 g)$^{-1}$)	70.0	63.9	93.4	104.0	47.7	25.0, 35.0	85.8
Stern coefficient, f_{Stern}	0.85	0.85	0.85	0.85	0.85	0.85	0.85

Note: LQB, low-quality bentonite; HQB, high-quality bentonite.

Table 10. Range of state, fabric and performance parameters of bentonites whose microstructure was experimentally investigated through indirect methods (hydraulic conductivity tests).

	Jo et al. (2004)	Lee and Shackelford (2005)	Katsumi et al. (2008)	Shackelford et al. (2016)	Ewy (2017)	Petrov and Rowe (1997)
Hydraulic conductivity, k ($m \cdot s^{-1}$)	5.1×10^{-11}	7.0×10^{-12}	5.8×10^{-12}	9.0×10^{-12}	2.9×10^{-16}	4.8×10^{-12}
	1.9×10^{-10}	2.4×10^{-11}	2.2×10^{-11}	—	7.4×10^{-14}	2.9×10^{-9}
Steric tortuosity factor, τ_m	—	—	—	0.092	—	—
Total void ratio, e	4.29	4.47	3.89	3.76	0.15	1.60
	6.58	4.87	5.14	—	0.40	4.89
Micro-void ratio, e_m	3.24	2.58	2.32	2.45	0.01	0.65
	5.03	3.51	3.09	—	0.23	3.82
Effective diffusion coefficient, D_s^* ($m^2 \cdot s^{-1}$)	—	—	—	1.83×10^{-10}	—	—
Effective specific surface, S_{eff} ($m^2 \cdot g^{-1}$)	64.61	186.54	116.88	146.60	3.50	16.17
	196.51	240.67	339.28	—	28.41	123.08
Average number of platelets per tactoid, $N_{l,AV}$	3.2	2.9	2.1	4.4	8.8	6.1
	9.6	3.3	7.5	—	71.41	46.4
Solid skeleton effective electric charge concentration, $\bar{c}_{sk,0}$ ($mol \cdot L^{-1}$)	0.030	0.091	0.059	0.070	0.002	0.007
	0.092	0.119	0.160	—	0.014	0.057

Table 11. Intrinsic parameters of bentonites whose microstructure was experimentally investigated through indirect methods (anion exclusion tests).

	Muurinen et al. (1989, 2013)	Van Loon et al. (2007)
Liquid limit, LL (%)	—	—
Plasticity index, PI (%)	—	—
Specific gravity, G_s	2.75	2.80
Total specific surface ($m^2 \cdot g^{-1}$)	610	560
Principal minerals (%)		
Montmorillonite	83.5	64.0
Mixed-layer illite–smectite	0.7	7.0
Quartz	2.8	4.0
Other	—	—
Cation exchange capacity, CEC (meq·(100 g)$^{-1}$)	84.0	76.0 120.0
Stern coefficient, f_{Stern}	0.85	0.85

Table 12. Range of state, fabric, and performance parameters of bentonites whose microstructure was experimentally investigated through indirect methods (anion exclusion tests).

	Muurinen et al. (1989)	Van Loon et al. (2007)	Muurinen et al. (2013)
Total void ratio, e	0.69	0.47	0.72
	1.71	1.15	2.93
Micro-void ratio, e_m	0.10	0.04	0.16
	0.73	0.38	1.70
Effective diffusion coefficient, D_s^* ($m^2 \cdot s^{-1}$)	—	—	—
Anion accessible porosity, n^*	0.024	0.002	0.050
	0.267	0.170	0.370
Effective specific surface, S_{eff} ($m^2 \cdot g^{-1}$)	22.05	9.03	44.06
	105.13	58.05	111.65
Average number of platelets per tactoid, $N_{l,AV}$	5.9	9.6	5.4
	28.2	62.0	13.8
Solid skeleton effective electric charge concentration, $\bar{c}_{sk,0}$ ($mol \cdot L^{-1}$)	0.011	0.004	0.021
	0.051	0.029	0.054

ically predicted CEC based on the available K^+. A blank test (performed without soil and using a 1 $mol \cdot L^{-1}$ KCl solution) showed that the NH_4^+ residue in the apparatus at most accounts for 1.3 meq·(100 g^{-1}). Therefore, the measured CEC suggests a release of NH_4^+ from the clay that is not related to the adsorption of K^+. According to the test method, washing the clay with isopropanol should remove the excess unbound ammonium acetate. However, the test results suggest that residual NH_4^+ remains in the clay. A replicate test was performed using 2.5 $mmol \cdot L^{-1}$ KCl and a double wash with isopropanol (240 mL instead of 120 mL), but no signif-

Fig. 15. Calibration of parameters that define FBS on experimental results given by Petrov and Rowe (1997) ($N_{1,AV0} = 1.56$, $\alpha = 8.82$, $\beta = 10.01$): (*a*) $N_{1,AV}$ versus e_m; (*b*) $N_{1,AV}$ versus c_s; (*c*) $N_{1,AV}$ versus c_s.

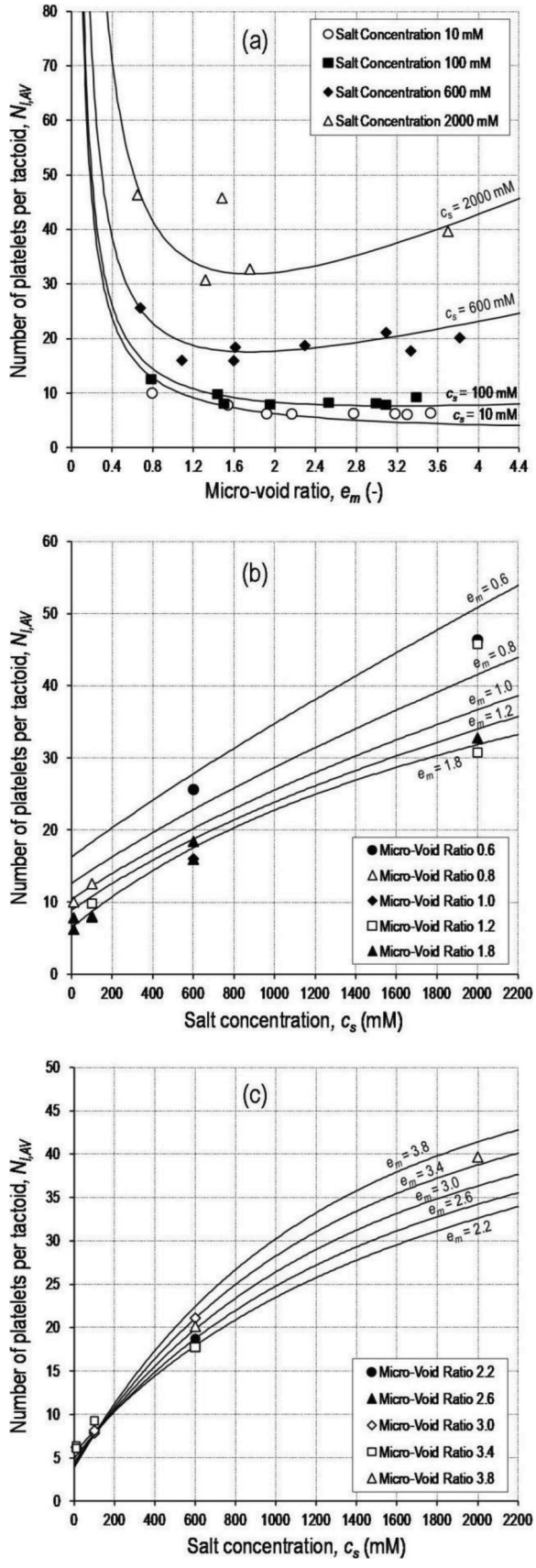

Fig. 16. Experimental versus theoretical average number of lamellae per tactoid, $N_{1,AV}$, using hydraulic conductivity data provided by Petrov and Rowe (1997) and related calibration of FBS parameters.

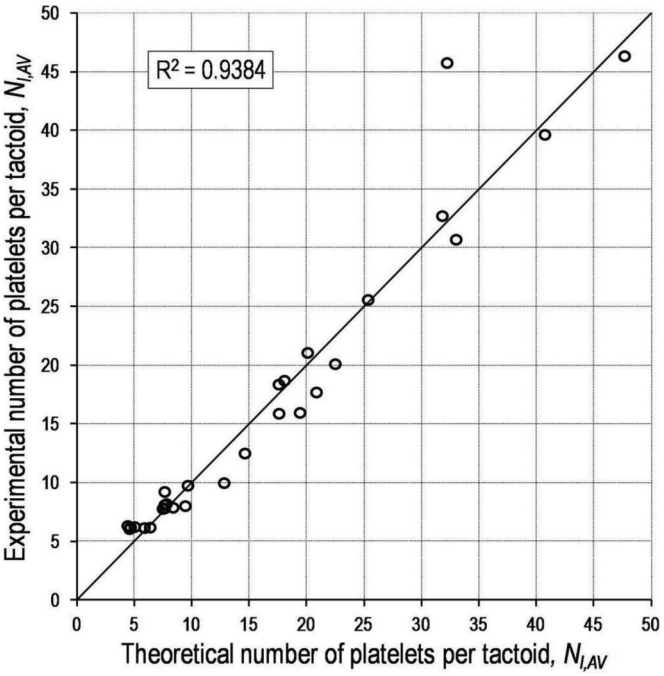

icant difference in the measured CEC was observed (Table 13). Therefore, the test results suggest that, even after washing with isopropanol, some unbound NH_4^+ remains entrapped in the bentonite layer. Filtration with low concentration (<20 mmol·L^{-1} KCl) solutions induces a change in bentonite fabric during the test, namely swelling and reorganization, whereby the release of NH_4^+ is favoured. At the macroscopic scale, this effect is reflected in the decrease in hydraulic conductivity of the bentonite, which resulted in a significantly longer duration of the final filtration stage at low or zero KCl concentrations, and an increase in the final height of the bentonite (about 8 mm with DW versus 2.5 mm with 1 mol·L^{-1} KCl).

Discussion

For a full and comprehensive understanding of the proposed interpretation of the unexpected results obtained from the aforementioned modified CEC tests, reference to the simplified scenario of a bentonite micropore and the related fluids and solutes depicted in Fig. 18 is useful. Such a simplified, conceptual scheme allows one to have an intuitive idea about the anion and cation concentration proportions, which refer to both the solid- and liquid-phase volumes involved in the chemico–physical exchange phenomena that occur during the standard ADM test for the CEC determination.

The sketch shown in Fig. 18 illustrates the typical proportions of the different ion concentrations at different distances from the bentonite particle surfaces. After washing with isopropanol, the remaining NH_4^+ cations are those that are able to electrically balance the negative surface charges of the lamellae surface. The unremoved NH_4^+ can be separated into two groups: the first group includes the Stern layer cations (the most tightly bonded to the solid phase) and the second group includes the residual cations of the DDL (weakly bonded to the solid phase), which can be identified as complementary to the Stern fraction. The electroneutrality requirement in the pore solution has been assumed for all the CEC determination test phases.

Table 13. Results of CEC determination by the ammonium displacement method, with both standard and nonstandard potassium chloride concentrations, and the methylene blue titration method.

Extracting KCl solution concentration	Estimated bentonite void ratio, e^a	Test 1 (meq·(100 g)$^{-1}$)	Test 2 (meq·(100 g)$^{-1}$)	Test 3 (meq·(100 g)$^{-1}$)	Notes
Ammonium displacement method[b]					
DW	14	17.5	20.4	13.9	—
1 mmol·L^{-1}	12	18.9	—	—	—
2.5 mmol·L^{-1}	12	21.4	17.7	—	—
		21.5	—	—	Double wash with isopropanol
10 mmol·L^{-1}	10	23.9	18.4	—	—
25 mmol·L^{-1}	8	42.0	45.4	—	—
50 mmol·L^{-1}	7	60.0	63.4	—	—
100 mmol·L^{-1}	6	76.2	74.4	103	—
1 mol·L^{-1} (standard)	4	73.2	60.7	—	—
		1.3	—	—	Blank test (no soil)
4.5 mol·L^{-1}	3	63.0	76.3	—	—
Methylene blue method[c]					
—	—	97.4	104	—	—

[a]Total void ratio estimated from the detection of the bentonite layer thickness within ceramic Buchner funnel at end of ammonium displacement tests.
[b]ASTM (2010) D7035, standard and modified procedure.
[c]EUBA (2002).

Fig. 17. Cation exchange capacity (CEC) values determined by ADM with different extracting KCl solution concentrations in final testing phase, and comparison with results obtained by MBM.

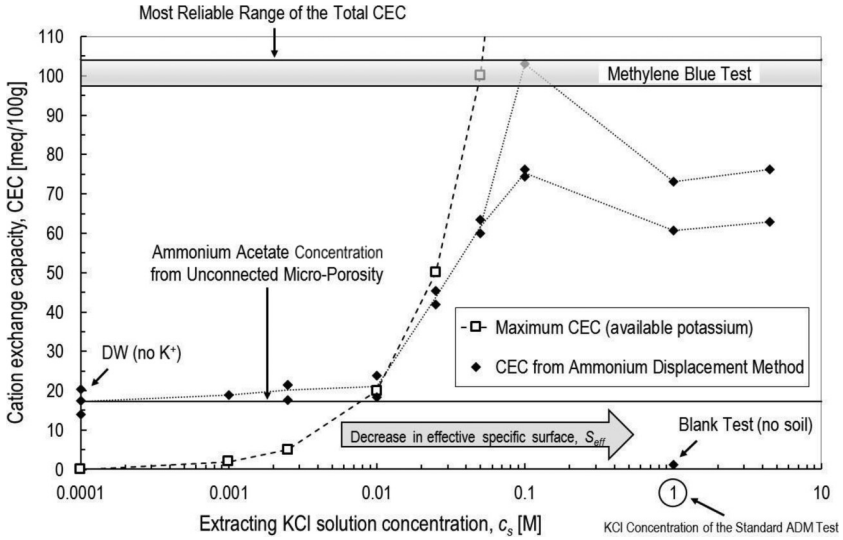

Although a sufficient number of experimental data are not available for the tested bentonite to determine the FBS parameters, a qualitative analysis can be addressed by using the input parameters obtained from the Petrov and Rowe (1997) hydraulic conductivity tests on a needle-punched GCL that resulted in $N_{l,AV0}$ = 1.56, α = 8.82, and β = 10.01, as illustrated previously (see Fig. 15).

During the isopropanol washing phase, the total void ratio was estimated, from the measurement of the bentonite layer thickness, to be about 4 and, as a result, $N_{l,AV}$ is calculated through the FBS equation to be about 4.74, assuming c_s = 0 as a consequence of the complete removal of the pore aqueous solution.

The relation between $N_{l,AV}$ and KCl concentration, c_s, provided by the FBS for the values of the bentonite void ratio that were estimated at the end of the ammonium displacement tests (Table 13) is shown in Fig. 19. The value of the KCl concentration corresponding to $N_{l,AV}$ = 4.74 is equal to about 27 mmol·L^{-1}. As a result, the bentonite is expected to swell during the KCl solution filtration phase and assume a more dispersed fabric when the KCl concentration is lower than 27 mmol·L^{-1}, whereas the bentonite is expected to flocculate and assume a more aggregated fabric when the KCl concentration is higher than 27 mmol·L^{-1}. Such a theoretical threshold KCl concentration is very close to the experimentally determined KCl concentration of 20 mmol·L^{-1}, below which the released NH_4^+ overcomes the available K^+ and above which the NH_4^+ seems to not be able to balance all the K^+ theoretically necessary to saturate the negative surface charge of a fully dispersed bentonite.

This quantitative comparison suggests a further complementary interpretation for the CEC data that were obtained from the NH_4^+ release measurements. After the washing phase with isopropanol, a portion of mobile NH_4^+ was not removed because of the presence of pores that are less accessible to advective flux, also referred to in the literature as dead-end and occluded pores (Shackelford and Moore 2013). When the KCl concentration of the extracting solution was lower than about 20 mmol·L^{-1}, the dispersion of the bentonite allowed the mobile NH_4^+ to be released by opening such pores. In contrast, when the KCl concentration of the extracting solution was higher than about 20 mmol·L^{-1}, the bentonite further flocculated by creating additional less accessible pore voids. The K^+ only had access to a limited portion of the

Fig. 18. Sketch of typical proportions of cation and anion concentrations at different distances from negatively charged surface of lamellae with reference to standard ADM for CEC determination.

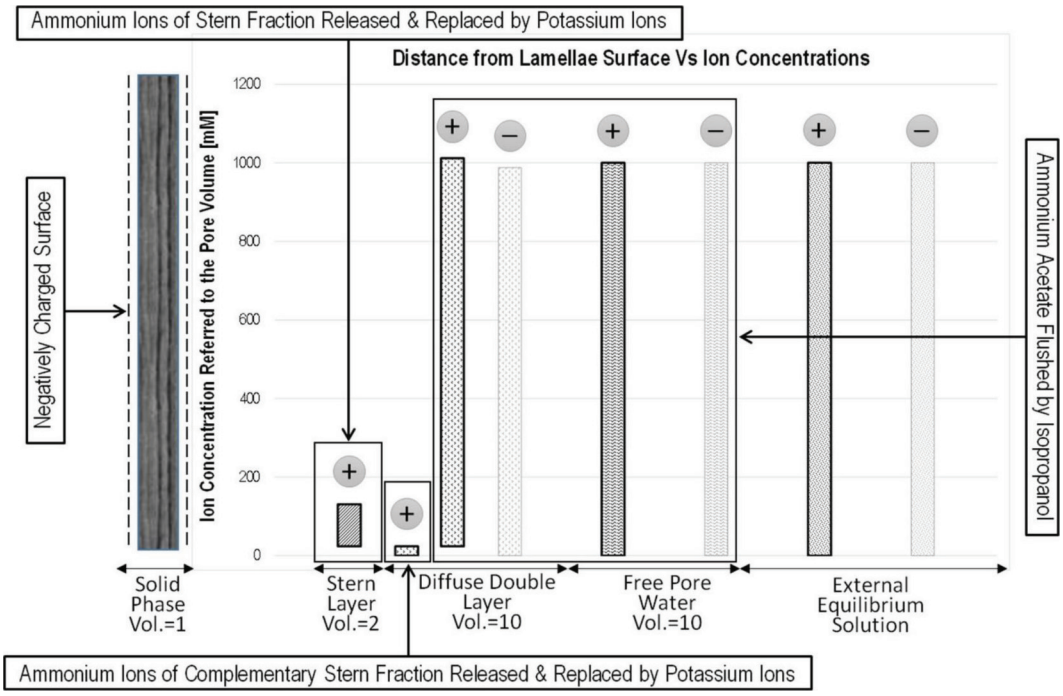

Fig. 19. Average number of lamellae per tactoid of bentonite as a function of the extracting KCl solution concentration. Arrows indicate KCl concentration that corresponds to $N_{l,AV}$ = 4.74, i.e., average number of lamellae per tactoid after isopropanol washing phase.

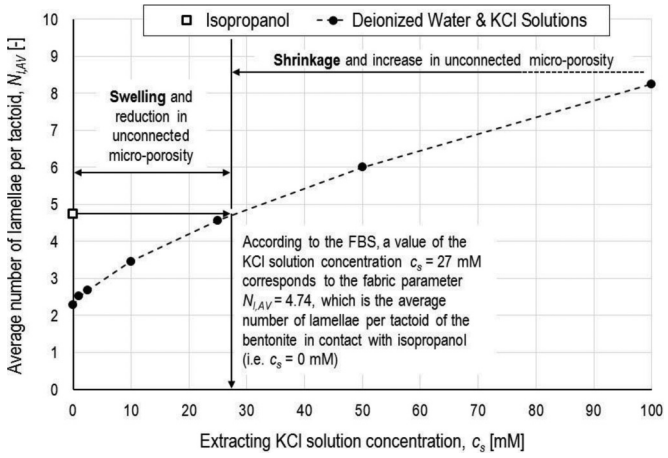

available pores for the highest concentrations of KCl (≥1 mol·L^{-1}), and the exchanged NH_4^+ measurements underestimated the effective bentonite CEC.

Finally, the peak value in the CEC provided from the measurement of the release of NH_4^+, at a KCl concentration equal to 0.1 mol·L^{-1}, could also be explained as the effect of two opposite trends, i.e., the increasing availability of K^+ for the exchange with NH_4^+ produced an increment in the release of NH_4^+, whereas the bentonite particle flocculation resulted in a reduction in the effective specific surface and in the bentonite exchange sites accessible to K^+, thus causing a decrease in the release of NH_4^+.

Again referring to the higher KCl concentrations (i.e., >100 mmol·L^{-1}), the post-peak CEC asymptotic trend versus KCl concentration seems to be supported and confirmed by a similar trend of the fabric parameter e_m. In fact, Fig. 20 shows a monotonic decrease in e_m, which has in turn been assessed from the interpretation of the experimental values of the total void ratio (Table 13) through the FBS (eqs. (35) and (36)), until a horizontal asymptote is approached for c_s > 0.1 mol·L^{-1}.

In summary, the tests performed by varying the KCl concentrations showed that the CEC measurements based on NH_4^+ release are influenced by bentonite fabric modifications and may provide an underestimation of the effective density of the sites available for cation exchange of a perfectly dispersed bentonite. For this reason, the ammonium displacement method does not seem to be sufficiently accurate to assess the fundamental fabric parameters of coupled hydrochemomechanical models, such as the one proposed in this paper. The MBM, which is used by industry for routine quality controls, seems to be able to provide a more reliable estimation of CEC, despite its apparently more limited accuracy, as the bentonite fabric is maintained dispersed during the test.

Conclusions

Within the field of unsaturated soil mechanics, resistance and deformability of a given fine-grained soil are governed primarily by the void ratio and effective confining stress. However, the degree of saturation and the related soil microfabric or structure play an even more important role in determining the mechanical behaviour of the fine-grained soil.

Similarly, the performance of bentonite-based barriers used for subsoil pollutant control, under fully saturated conditions, is also governed by the ion valence and concentration of solutes in the pore solution and the related microfabric or structure. In this case the barrier performances can be expressed in terms of hydraulic conductivity, diffusivity, osmotic efficiency, and swelling properties.

As bentonite particles can be considered as infinitely extended platy particles (platelets or lamellae), they can have a dispersed structure or fabric in which clay particles are present as well-separated units or as an aggregated structure that consists of packets of particles, or tactoids, within which several clay platelets are in a parallel array. The formation of tactoids has the net

Fig. 20. Ranges of main and minor microporosity variation versus KCl solution concentration and related boundary concentration value. Aforementioned ranges have to be compared with CEC trend that was obtained by the ADM at different KCl solution concentrations.

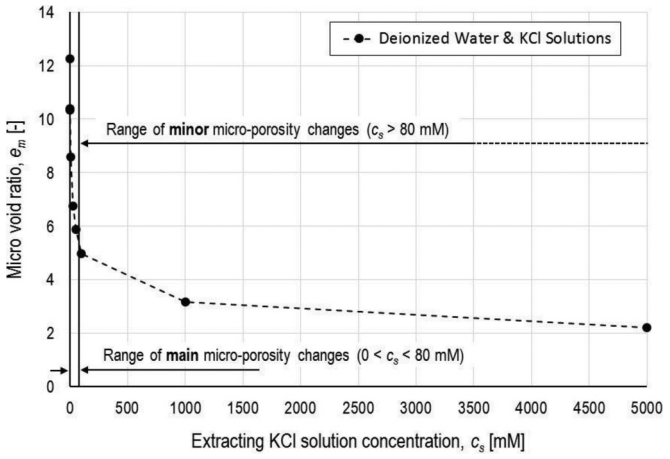

result of reducing the surface area of the montmorillonite, which then behaves like a much larger, aggregated particle with the negative electrical charges being fully manifested on the outside surfaces and, therefore, the only charges capable of interacting with the mobile portion of the pore fluid and related ions in solution.

Referring to this very simple but fully realistic conceptual geometry, an effective fabric parameter referred to as the average number of lamellae per tactoid, $N_{l,AV}$, has been defined. This fabric parameter allows quantification in a very direct and clear manner of the microfabric or structure of the bentonite. Moreover, $N_{l,AV}$ can be directly linked with the external or effective specific surface of the tactoids, S_{eff}, through the total specific surface of the single lamellae, S, and in turn with the average distances between tactoids and between the lamellae of the single tactoid together with the related micro, e_m, and nano, e_n, void ratios. Based on this conceptual framework, derivation of the other electrochemical intrinsic and fabric parameters of the considered bentonite, such as the solid skeleton effective electric charge concentration, $\bar{c}_{sk,0}$, the Stern fraction, f_{Stern}, and related Stern layer thickness, d_{Stern}, is possible.

Through the use of the aforementioned intrinsic and fabric parameters that characterize the solid phase of bentonite, a theoretical model, capable of linking the coupled transport phenomena of water and ions by imposing the chemical equilibrium between the bulk electrolyte solutions and the internal micropore solution at the macroscopic scale level — through the Donnan, Navier–Stokes, and Nernst–Planck equations — can be implemented. Moreover, the same model allows for the assessment of the osmotic component of the swelling pressure, u_{sw}, which, when introduced within the original effective stress principle of Terzaghi (1943), makes it possible to define a general relationship among the microvoid ratio, e_m, the electrolyte concentration, c_s, and the average number of lamellae per tactoid for any given bentonite by simply taking into account the stress–strain equilibrium and compatibility within the porous medium. Within the 3D domain, identified by the micro-void ratio, e_m, the electrolyte concentration, c_s, and the average number of lamellae per tactoid, $N_{l,AV}$, this relationship takes the shape of a surface referred to as the fabric boundary surface (FBS).

Due to the complex mathematics of the aforementioned FBS derivation and related use, an approximate solution has been developed to generalize and facilitate the application of the proposed model. This solution has been used for the validation of the proposed framework and related theoretical models through comparison between theoretical predictions in terms of $N_{l,AV}$ versus experimental results obtained from both direct (NMR, XRD, SAXS, TEM) and indirect (hydraulic conductivity, swelling, osmosis, anion available pore volume) experimental techniques.

The first two series of experimental results refer to six different sodium bentonites with smectite contents greater than 70%, which were used to define the three parameters that characterize the simplified version of the FBS, i.e., the ideal average minimum number of lamellae per tactoid, $N_{l,AV0}$, the coefficient α relating $N_{l,AV}$ and e_m when $c_s = 0$, and the constriction coefficient β that accounts for the possible movements of lamellae versus void ratio due to mechanical constraints. Moreover, a third series of tests involving nine other sodium bentonites, all with more than 64% smectite content, was used for the final validation of the proposed theoretical model.

Apart from a small segment of the test results that are suspect due to a series of uncertainties resulting from the questionable reliability of the experimental technique and related interpretation procedure, in particular, when reference is made specifically to the basic fabric parameter (i.e., $N_{l,AV}$), the agreement between the majority of the experimental results versus the theoretical predictions is more than satisfactory. Such a good agreement is particularly noteworthy in light of the different experimental techniques (i.e., direct and indirect methods), the different types of phenomenological parameters to be assessed, the different laboratories and research groups, and the different time periods associated with the considered test results.

When the parameters characterizing the FBS of a single bentonite and (or) GCL were determined only on the basis of tests conducted on the specific material, such as has been done in the case of the numerous series of hydraulic conductivity tests on a GCL from Petrov and Rowe (1997), all the theoretical results predicted by the proposed model can be considered very good.

Among the three main categories of input data, i.e., intrinsic, state, and fabric parameters, which have to be determined for an appropriate and reliable use of the proposed theoretical model, an important role is played by the basic intrinsic parameters and, in particular, by the cation exchange capacity, CEC, and the Stern fraction, f_{Stern}. These parameters have been observed to vary in a rather narrow range for clays with montmorillonite contents over 60%. Nevertheless, the results of a series of laboratory tests conducted to investigate the reliability of the standard procedure for the CEC assessment illustrated a significant underestimation of CEC due to the significant influence of the clay fabric at the high KCl concentration (i.e., 1 mol·L^{-1}) that is specified by the standard ammonium displacement method (ADM). In contrast, the methylene blue titration method (MBM), which is used by industry for routine quality controls, seems to provide a more reliable estimation of CEC, despite an apparently more limited accuracy, as the bentonite fabric is maintained dispersed during the entire testing procedure.

In summary, the proposed theoretical framework and related hydrochemicomechanical models appear capable of estimating the performance of bentonite-based barriers for subsoil pollutant control in terms of hydraulic conductivity, k, osmotic efficiency, ω, and osmotic swelling pressure, u_{sw}, once the intrinsic chemicophysical parameters (i.e., ρ_{sk}, S, σ, d_{Stern}, and f_{Stern}) are known together with the chemicomechanical state and fabric parameters (i.e., c_s, e, e_m, e_n, $N_{l,AV}$, and $\bar{c}_{sk,0}$).

Regardless of the validation of the proposed theoretical framework evidenced in this study, additional evaluation is still needed to improve the aforementioned theoretical predictions together with the reliability of the experimental results. In particular, two issues are worth noting:

- From the experimental viewpoint, improvement of the existing techniques and implementation of new methods for a more reliable determination of some of the basic intrinsic parame-

ters in bentonites (e.g., CEC and f_{Stern}) and for the assessment of their nano- and microfabric (e.g., $N_{l,AV}$ and S_{eff}) are needed.
- From the point of view of the proposed theoretical model, a better definition of the roles played on the bentonite nano- and microfabric by both the stress–strain history and the electrolyte exposure history in terms of concentration and ion valence is needed.

Finally, extension of the theoretical framework and model to transition from fully saturated conditions to partially saturated conditions is a longer term goal.

Acknowledgements

The author would like to express his gratitude to the Members of the Technical Committee TC215 of ISSMGE for choosing the author to deliver the second R. Kerry Rowe Lecture, which is considered as one of the highest honours within the entire international geotechnical community. The author is also grateful to ENI S.p.A., Milan (Italy), for financing the research activity on bentonites carried out at the geotechnical laboratory of the Politecnico di Torino (Italy). Moreover, there are two colleagues, in particular, that have made this work possible: Andrea Dominijanni from Politecnico di Torino (Italy) and Charles D. Shackelford from Colorado State University (USA). Their direct cooperation, stimulating discussions, and valuable support are deeply recognized and appreciated by the author. The author also wishes to acknowledge and thank staff from Geotechnical-Engineering professional firm, Torino (Italy), and colleagues of the geotechnical research groups of Politecnico di Torino (Italy), École Polytechnique Fédérale de Lausanne (Switzerland), and Università Politecnica delle Marche, Ancona (Italy) for their assistance and support. Finally, a special thanks to former Ph.D. student, Giacomo Boffa, and to candidate Ph.D. graduate student, Nicolò Guarena, for their cooperation in the preparation and editing of this paper.

References

Acikel, A.S., Gates, W.P., Singh, R.M., Bouazza, A., and Rowe, R.K. 2018. Insufficient initial hydration of GCLs from some subgrades: factors and causes. Geotextiles and Geomembranes, **46**(6): 770–781. doi:10.1016/j.geotexmem.2018.06.007.

Alonso, E., Gens, A., and Josa, A. 1990. A constitutive model for partially saturated soils. Géotechnique, **40**(3): 405–430. doi:10.1680/geot.1990.40.3.405.

Altmann, S. 2008. Geochemical research: a key building block for nuclear waste disposal safety cases. Journal of Contaminant Hydrology, **102**(3–4): 174–179. doi:10.1016/j.jconhyd.2008.09.012. PMID:19008019.

Altmann, S., Tournassat, C., Goutelard, F., Parneix, J.C., Gimmi, T., and Maes, N. 2012. Diffusion-driven transport in clayrock formations. Applied Geochemistry, **27**(2): 463–478. doi:10.1016/j.apgeochem.2011.09.015.

Andra. 2005. Référentiel du comportement des radionucléides et des toxiques chimiques d'un stockage dans le Callovo-Oxfordien jusqu'à l'Homme. Dossier 2005 Argile. Agence Nationale pour la gestion des déchets radioactifs, Châtenay-Malabry, France.

ASTM. 2010. Standard test method for measuring the exchange complex and cation exchange capacity of inorganic fine-grained soils. ASTM standard D7503-10. ASTM International, West Conshohocken, Pa.

Birgersson, M., and Karnland, O. 2009. Ion equilibrium between montmorillonite interlayer space and an external solution–Consequences for diffusional transport. Geochimica et Cosmochimica Acta, **73**(7): 1908–1923. doi:10.1016/j.gca.2008.11.027.

Bock, H., Dehandschutter, B., Martin, C.D., Mazurek, M., De Haller, A., Skoczylas, F., and Davy, C. 2010. Self-sealing fractures in argillaceous formations in the context of geological disposal of radioactive waste. Nuclear Energy Agency, Organisation for Economic Co-operation and Development.

Boffa, G. 2016. Mechanical and transport phenomena in advanced pollutants containment systems. Ph.D. thesis, Department of Structural, Geotechnical and Building Engineering, Politecnico di Torino, Torino, Italy.

Bolt, G.H. 1956. Physico-chemical analysis of the compressibility of pure clays. Géotechnique, **6**(2): 86–93. doi:10.1680/geot.1956.6.2.86.

Bolt, G.H., and de Haan, F.A.M. 1982. Anion exclusion in soils. *In* Soil chemistry: B. Physico-chemical models. *Edited by* G.H. Bolt. Elsevier, Amsterdam, Netherlands. pp. 233–257.

Borgia, G.C., Brown, R.J.S., and Fantazzini, P. 1998. Uniform-penalty inversion of multiexponential decay data. Journal of Magnetic Resonance, **132**(1): 65–77. doi:10.1006/jmre.1998.1387. PMID:9615412.

Bourg, I.C., Sposito, G., and Bourg, A.C.M. 2006. Tracer diffusion in compacted, water-saturated bentonite. Clays and Clay Minerals, **54**(3): 363–374. doi:10.1346/CCMN.2006.0540307.

Carman, P.C. 1956. Flow of gases through porous media. Butterworths, London (UK).

Delay, J., Vinsot, A., Krieguer, J.M., Rebours, H., and Armand, G. 2007. Making of the underground scientific experimental programme at the Meuse/Haute-Marne underground research laboratory, North Eastern France. Physics and Chemistry of the Earth, Parts A/B/C, **32**(1–7): 2–18. doi:10.1016/j.pce.2006.04.033.

Di Emidio, G. 2010. Hydraulic and chemico-osmotic performance of polymer treated clays. Ph.D. thesis, Department of Civil Engineering, Ghent University, Ghent, Belgium.

Dominijanni, A., and Manassero, M. 2005. Modelling osmosis and solute transport through clay membrane barriers. *In* Proceedings of the Geo-Frontiers Congress, Austin, Texas (USA), 24–26 January 2005. *Edited by* A. Alshawabkleh, C.H. Benson, P.J. Culligan, J.C. Evans, B.A. Gross, D. Narejo, et al. American Society of Civil Engineers, Reston, Virginia, USA. pp. 349–360.

Dominijanni, A., and Manassero, M. 2008. Modeling the compressibility and the hydraulic conductivity of geosynthetic clay liners. *In* Proceedings of the First Pan American Geosynthetics Conference & Exhibition, Cancun, Mexico, 2–5 March 2008. pp. 59–68.

Dominijanni, A., and Manassero, M. 2012*a*. Modelling the swelling and osmotic properties of clay soils. Part I: the phenomenological approach. International Journal of Engineering Science, **51**: 32–50. doi:10.1016/j.ijengsci.2011.11.003.

Dominijanni, A., and Manassero, M. 2012*b*. Modelling the swelling and osmotic properties of clay soils. Part II: the physical approach. International Journal of Engineering Science, **51**: 51–73. doi:10.1016/j.ijengsci.2011.11.001.

Dominijanni, A., Manassero, M., and Vanni, D. 2006. Micro/macro modeling of electrolyte transport through semipermeable bentonite layers. *In* Proceedings of the 5th International Congress on Environmental Geotechnics, Cardiff, Wales, UK, 26–30 June 2006. *Edited by* H.R. Thomas. Thomas Telford, London, UK. Vol. 2, pp. 1123–1130.

Dominijanni, A., Manassero, M., and Puma, S. 2013. Coupled chemical-hydraulic-mechanical behaviour of bentonites. Géotechnique, **63**(3): 191–205. doi:10.1680/geot.SIP13.P.010.

Dominijanni, A., Manassero, M., Boffa, G., and Puma, S. 2017. Intrinsic and state parameters governing the efficiency of bentonite barriers for contaminant control. *In* Proceedings of the International Workshop on Advances in Laboratory Testing and Modelling of Soils and Shales, Villars-sur-Ollon, Switzerland, 18–20 January 2017. *Edited by* A. Ferrari and L. Laloui. Springer International Publishing AG, Cham, Switzerland. pp. 45–56.

Dominijanni, A., Guarena, N., and Manassero, M. 2018. Laboratory assessment of semi-permeable properties of a natural sodium bentonite. Canadian Geotechnical Journal, **55**(11): 1611–1631. doi:10.1139/cgj-2017-0599.

EUBA. 2002. Methodology for the determination of the methylene blue value of bentonite. European Bentonite Association.

Ewy, R.T. 2017. Shale capillarity, osmotic suction and permeability, and solutions to practical testing issues. *In* Proceedings of the International Workshop on Advances in Laboratory Testing and Modelling of Soils and Shales, Villars-sur-Ollon, Switzerland, 18–20 January 2017. *Edited by* A. Ferrari and L. Laloui. Springer International Publishing AG, Cham, Switzerland. pp. 29–36.

García-Gutiérrez, M., Cormenzana, J.L., Missana, T., and Mingarro, M. 2004. Diffusion coefficients and accessible porosity for HTO and $^{36}Cl^-$ in compacted FEBEX bentonite. Applied Clay Science, **26**(1–4): 65–73. doi:10.1016/j.clay.2003.09.012.

Glaus, M.A., Baeyens, B., Bradbury, M.H., Jakob, A., Van Loon, L.R., and Yaroshchuk, A. 2007. Diffusion of ^{22}Na and ^{85}Sr in montmorillonite: evidence of interlayer diffusion being the dominant pathway at high compaction. Environmental Science & Technology, **41**(2): 478–485. doi:10.1021/es061908d. PMID:17310710.

Grim, R.E. 1962. Applied clay mineralogy. McGraw–Hill, New York.

Guyonnet, D., Gaucher, E., Gaboriau, H., Pons, C.H., Clinard, C., Norotte, V., and Didier, G. 2005. Geosynthetic clay liner interaction with leachate: correlation between permeability, microstructure, and surface chemistry. Journal of Geotechnical and Geoenvironmental Engineering, **131**(6): 740–749. doi:10.1061/(ASCE)1090-0241(2005)131:6(740).

Guyonnet, D., Touze-Foltz, N., Norotte, V., Pothier, C., Didier, G., Gailhanou, H., et al. 2009. Performance-based indicators for controlling geosynthetic clay liners in landfill applications. Geotextiles and Geomembranes, **27**(5): 321–331. doi:10.1016/j.geotexmem.2009.02.002.

Ichikawa, Y., Kawamura, K., Fujii, N., and Kitayama, K. 2004. Microstructure and micro/macro-diffusion behavior of tritium in bentonite. Applied Clay Science, **26**(1–4): 75–90. doi:10.1016/j.clay.2003.09.013.

Järvinen, J., Matusewicz, M., and Itälä, A. 2016. Methodology for studying the composition of non-interlamellar pore water in compacted bentonite. Clay Minerals, **51**(2): 173–187. doi:10.1180/claymin.2016.051.2.05.

Jo, H.Y., Benson, C., and Edil, T. 2004. Hydraulic conductivity and cation exchange in non-prehydrated and prehydrated bentonite permeated with weak inorganic salt solutions. Clays and Clay Minerals, **52**(6): 661–679. doi:10.1346/CCMN.2004.0520601.

Kaczmarek, M., and Hueckel, T. 1998. Chemo-mechanical consolidation of clays: analytical solutions for a linearized one-dimensional problem. Transport in Porous Media, **32**(1): 49–74. doi:10.1023/A:1006530405361.

Karnland, O., Muurinen, A., and Karlsson, F. 2005. Bentonite swelling pressure in NaCl solutions–Experimentally determined data and model calculations. *In* Proceedings of Advances in Understanding Engineered Clay Barriers, Barcelona, Spain, 12–14 November 2003. *Edited by* E. Alonso and A. Ledesma. Taylor & Francis Group, London, UK. pp. 241–256.

Katchalsky, A., and Curran, P.F. 1965. Nonequilibrium thermodynamics in biophysics. Harvard University Press, Cambridge, Mass.

Kato, H., Muroi, M., Yamada, N., Ishida, H., and Sato, H. 1995. Estimation of effective diffusivity in compacted bentonite. *In* Proceedings of the 18th International Symposium on the Scientific Basis for Nuclear Waste Management, Kyoto, Japan, 23–27 October 1994. *Edited by* T. Murakami and R.C. Ewing. Materials Research Society, Pittsburgh, Pa. pp. 277–284.

Katsumi, T., Ishimori, H., Onikata, M., and Fukagawa, R. 2008. Long-term barrier performance of modified bentonite materials against sodium and calcium permeant solutions. Geotextiles and Geomembranes, **26**(1): 14–30. doi:10.1016/j.geotexmem.2007.04.003.

Kozeny, J. 1927. Ueber kapillare Leitung des Wassers im Boden. Sitzungsber Akad. Wiss., Wien, **136**(2a): 271–306.

Laird, D.A. 2006. Influence of layer charge on swelling of smectites. Applied Clay Science, **34**(1–4): 74–87. doi:10.1016/j.clay.2006.01.009.

Laird, D.A., Thompson, M.L., and Scott, A.D. 1989. Technique for transmission electron microscopy and X-ray powder diffraction analyses of the same clay mineral specimen. Clays and Clay Minerals, **37**(3): 280–282. doi:10.1346/CCMN.1989.0370313.

Lee, J.M., and Shackelford, C.D. 2005. Impact of bentonite quality on hydraulic conductivity of geosynthetic clay liners. Journal of Geotechnical and Geoenvironmental Engineering, **131**(1): 64–77. doi:10.1061/(ASCE)1090-0241(2005)131:1(64).

Leroy, P., Revil, A., and Coelho, D. 2006. Diffusion of ionic species in bentonite. Journal of Colloid and Interface Science, **296**(1): 248–255. doi:10.1016/j.jcis.2005.08.034. PMID:16154580.

Likos, W.J., Bowders, J.J., and Gates, W.P. 2010. Mineralogy and engineering properties of bentonite. *In* Geosynthetic clay liners for waste containment facilities. *Edited by* A. Bouazza and J.J. Bowders. CRC Press/Balkema, Taylor & Francis Group, London, UK. pp. 31–53.

Malusis, M.A., and Shackelford, C.D. 2002*a*. Chemico-osmotic efficiency of a geosynthetic clay liner. Journal of Geotechnical and Geoenvironmental Engineering, **128**(2): 97–106. doi:10.1061/(ASCE)1090-0241(2002)128:2(97).

Malusis, M.A., and Shackelford, C.D. 2002*b*. Coupling effects during steady-state solute diffusion through a semipermeable clay membrane. Environmental Science & Technology, **36**(6): 1312–1319. doi:10.1021/es011130q. PMID:11944686.

Malusis, M.A., Shackelford, C.D., and Olsen, H.W. 2001. A laboratory apparatus to measure chemico-osmotic efficiency coefficients for clay soils. Geotechnical Testing Journal, **24**(3): 229–242. doi:10.1520/GTJ11343J.

Malusis, M.A., Kang, J.B., and Shackelford, C.D. 2013. Influence of membrane behavior on solute diffusion through GCLs. *In* Proceedings of the International Symposium on Coupled Phenomena in Environmental Geotechnics, Torino, Italy, 1–3 July 2013. *Edited by* M. Manassero, A. Dominijanni, S. Foti, and G. Musso. CRC Press/Balkema, Taylor & Francis Group, London, UK. pp. 267–274.

Manalo, F.P., Kantzas, A., and Langford, C.H. 2003. Soil wettability as determined from using low-field nuclear magnetic resonance. Environmental Science & Technology, **37**(12): 2701–2706. doi:10.1021/es0259685. PMID:12854708.

Manassero, M. 2017. On the fabric and state parameters of active clays for contaminant control. *In* Proceedings of the 19th International Conference of Soil Mechanics and Geotechnical Engineering, Seoul, Korea, 17–22 September 2017. *Edited by* W. Lee, J.-S. Lee, H.-K. Kim, and D.-S. Kim. pp. 167–189.

Manassero, M., and Dominijanni, A. 2003. Modelling the osmosis effect on solute migration through porous media. Géotechnique, **53**(5): 481–492. doi:10.1680/geot.2003.53.5.481.

Manassero, M., and Dominijanni, A. 2010. Coupled modelling of swelling properties and electrolyte transport through geosynthetic clay liners. *In* Proceedings of the 6th International Congress on Environmental Geotechnics, New Delhi, India, 8–12 November 2010. *Edited by* M. Datta, R.K. Srivastava, G.V. Ramana, and J.T. Shahu. Tata McGraw Hill, New Delhi, India. Vol. 1, pp. 260–271.

Manassero, M., Dominijanni, A., Musso, G., and Puma, S. 2014. Coupled phenomena in contaminant transport. *In* Proceedings of the 7th International Congress on Environmental Geotechnics, Melbourne, Australia, 10–14 November 2014. *Edited by* A. Bouazza, S. Yuen, and B. Brown. Engineers Australia, Barton ACT, Australia. pp. 144–169.

Manassero, M., Dominijanni, A., Fratalocchi, E., Mazzieri, F., Pasqualini, E., and Boffa, G. 2016. About the state parameters of active clays. *In* Geoenvironmental Engineering: Honoring David E. Daniel, Chicago, Illinois (USA), 14–18 August 2016. *Edited by* C.H. Benson and C.D. Shackelford. Geotechnical Special Publication No. 274, American Society of Civil Engineers (ASCE). pp. 99–110.

Manca, D. 2015. Hydro-chemo-mechanical characterization of sand/bentonite mixtures, with focus on their water and gas transport properties. Ph.D. thesis, École polytechnique fédérale de Lausanne EPFL, Lausanne, Switzerland.

Matusewicz, M., Pirkkalainen, K., Liljeström, V., Suuronen, J.P., Root, A., Muurinen, A., et al. 2013. Microstructural investigation of calcium montmorillonite. Clay Minerals, **48**(2): 267–276. doi:10.1180/claymin.2013.048.2.08.

Mazzieri, F., and Di Emidio, G. 2011. Caratteristiche e prestazioni di geocompositi bentonitici preidratati. *In* Proceedings of the 24th Italian Geotechnical Conference, Napoli, Italy, 22–24 June 2011. Associazione Geotecnica Italiana (AGI), Roma, Italy. pp. 735–742. [In Italian.]

Mazzieri, F., Di Emidio, G., Fratalocchi, E., Di Sante, M., and Pasqualini, E. 2013. Permeation of two GCLs with an acidic metal-rich synthetic leachate. Geotextiles and Geomembranes, **40**: 1–11. doi:10.1016/j.geotexmem.2013.07.011.

Mitchell, J.K., and Soga, K. 2005. Fundamentals of soil behavior. 3rd ed. John Wiley and Sons, New York.

Mitchell, J., Webber, J.B.W., and Strange, J.H. 2008. Nuclear magnetic resonance cryoporometry. Physics Reports, **461**(1): 1–36. doi:10.1016/j.physrep.2008.02.001.

Molera, M., Eriksen, T., and Jansson, M. 2003. Anion diffusion pathways in bentonite clay compacted to different dry densities. Applied Clay Science, **23**(1–4): 69–76. doi:10.1016/S0169-1317(03)00088-7.

Montavon, G., Guo, Z., Tournassat, C., Grambow, B., and Le Botlan, D. 2009. Porosities accessible to HTO and iodide on water-saturated compacted clay materials and relation with the forms of water: a low field proton NMR study. Geochimica et Cosmochimica Acta, **73**(24): 7290–7302. doi:10.1016/j.gca.2009.09.014.

Musso, G., Cosentini, R.M., Dominijanni, A., Guarena, N., and Manassero, M. 2017. Laboratory characterization of the chemo-hydro-mechanical behaviour of chemically sensitive clays. Rivista Italiana di Geotecnica, **3**: 22–47.

Muurinen, A., Penttilä-Hilthunen, P., and Uusheimo, K. 1989. Diffusion of chloride and uranium in compacted sodium bentonite. *In* Proceedings of the 12th International Symposium on the Scientific Basis for Nuclear Waste Management, Berlin, Germany, 10–13 October 1988. *Edited by* W. Lutze and R.C. Ewing. Materials Research Society, Pittsburgh, Pennsylvania, USA. pp. 743–748.

Muurinen, A., Karnland, O., and Lehikoinen, J. 2004. Ion concentration caused by an external solution into the porewater of compacted bentonite. Physics and Chemistry of the Earth, Parts A/B/C, **29**(1): 119–127. doi:10.1016/j.pce.2003.11.004.

Muurinen, A., Karnland, O., and Lehikoinen, J. 2007. Effect of homogenization on the microstructure and exclusion of chloride in compacted bentonite. Physics and Chemistry of the Earth, Parts A/B/C, **32**(1–7): 485–490. doi:10.1016/j.pce.2006.02.058.

Muurinen, A., Carlsson, T., and Root, A. 2013. Bentonite pore distribution based on SAXS, chloride exclusion and NMR studies. Clay Minerals, **48**(2): 251–266. doi:10.1180/claymin.2013.048.2.07.

Norrish, K. 1954. The swelling of montmorillonite. Discussions of the Faraday Society, **18**: 120–134. doi:10.1039/df9541800120.

Ohkubo, T., Kikuchi, H., and Yamaguchi, M. 2008. An approach of NMR relaxometry for understanding water in saturated compacted bentonite. Physics and Chemistry of the Earth, Parts A/B/C, **33**: S169–S176. doi:10.1016/j.pce.2008.10.042.

Ohkubo, T., Ibaraki, M., Tachi, Y., and Iwadate, Y. 2016. Pore distribution of water-saturated compacted clay using NMR relaxometry and freezing temperature depression; effects of density and salt concentration. Applied Clay Science, **123**: 148–155. doi:10.1016/j.clay.2016.01.014.

Petrov, R.J., and Rowe, R.K. 1997. Geosynthetic clay liner (GCL) – chemical compatibility by hydraulic conductivity testing and factors impacting its performance. Canadian Geotechnical Journal, **34**(6): 863–885. doi:10.1139/t97-055.

Puma, S., Dominijanni, A., Manassero, M., and Zaninetta, L. 2015. The role of physical pretreatments on the hydraulic conductivity of natural sodium bentonites. Geotextiles and Geomembranes, **43**(3): 263–271. doi:10.1016/j.geotexmem.2015.02.001.

Pusch, R., Karnland, O., and Hökmark, H. 1990. GMM–a general microstructural model for qualitative and quantitative studies of smectite clays. SKB Technical Report 90-43, Swedish Nuclear Fuel and Waste Management Corporation, Stockholm, Sweden.

Quirk, J.P., and Aylmore, L.A.G. 1971. Domains and quasi-crystalline regions in clay systems. Soil Science Society of America Proceedings, **35**(4): 652–654. doi:10.2136/sssaj1971.03615995003500040046x.

Seiphoori, A. 2014. Thermo-hydro-mechanical characterization and modelling of MX-80 granular bentonite. Ph.D. thesis, École polytechnique fédérale de Lausanne EPFL, Lausanne, Switzerland.

Shackelford, C.D., and Moore, S.M. 2013. Fickian diffusion of radionuclides for engineered containment barriers: diffusion coefficients, porosities, and complicating issues. Engineering Geology, **152**(1): 133–147. doi:10.1016/j.enggeo.2012.10.014.

Shackelford, C.D., Benson, C.H., Katsumi, T., Edil, T.B., and Lin, L. 2000. Evaluating the hydraulic conductivity of GCLs permeated with non-standard liquids. Geotextiles and Geomembranes, **18**(2–4): 133–161. doi:10.1016/S0266-1144(99)00024-2.

Shackelford, C.D., Meier, A., and Sample-Lord, K. 2016. Limiting membrane and diffusion behavior of a geosynthetic clay liner. Geotextiles and Geomembranes, **44**(5): 707–718. doi:10.1016/j.geotexmem.2016.05.009.

Shainberg, I., Bresler, E., and Klausner, Y. 1971. Studies on Na/Ca montmorillonite systems. 1. The swelling pressure. Soil Science, **111**(4): 214–219.

SKB. 2011. Long-term safety for the final repository for spent nuclear fuel at Forsmark. Technical Report TR-11-01, Svensk Kärnbränslehantering AB, Swedish Nuclear Fuel and Waste Management Co, Stockholm, Sweden.

Skempton, A.W. 1961. Effective stress in soils, concrete and rocks. *In* Pore pressure and suction in soils. Butterworths, London, UK. pp. 4–16.

Spiegler, K.S., and Kedem, O. 1966. Thermodynamics of hyperfiltration (reverse osmosis): criteria for efficient membranes. Desalination, **1**(4): 311–326. doi:10.1016/S0011-9164(00)80018-1.

Terzaghi, K. 1936. The shearing resistance of saturated soil and the angle between the planes of shear. *In* Proceedings of the 1st International Conference on Soil Mechanics and Foundation Engineering, Cambridge, Massachusetts, 22–26 June 1936. Harvard Printing Office. Vol. 1, pp. 54–56.

Terzaghi, K. 1943. Theoretical soil mechanics. John Wiley and Sons, New York.

Tessier, D. 1990. Behavior and microstructure of clay minerals. *In* Soil colloids and their associations in aggregates. *Edited by* M.F. De Boodt, M.H.B. Hayes, and A. Herbillon. Plenum Press, New York. pp. 387–415.

Tinnacher, R.M., Holmboe, M., Tournassat, C., Bourg, I.C., and Davis, J.A. 2016. Ion adsorption and diffusion in smectite: molecular, pore, and continuum scale views. Geochimica et Cosmochimica Acta, **177**: 130–149. doi:10.1016/j.gca.2015.12.010.

Todoruk, T.R., Langford, C.H., and Kantzas, A. 2003. Pore-scale redistribution of water during wetting of air-dried soils as studied by low-field NMR relaxometry. Environmental Science & Technology, **37**(12): 2707–2713. doi:10.1021/es025967c. PMID:12854709.

Tournassat, C., and Appelo, C.A.J. 2011. Modelling approaches for anion-exclusion in compacted Na-bentonite. Geochimica et Cosmochimica Acta, **75**(13): 3698–3710. doi:10.1016/j.gca.2011.04.001.

Tournassat, C., Chapron, Y., Leroy, P., Bizi, M., and Boulahya, F. 2009. Comparison of molecular dynamics simulations with triple layer and modified Gouy-Chapman models in a 0.1M NaCl-montmorillonite system. Journal of Colloid and Interface Science, **339**(2): 533–541. doi:10.1016/j.jcis.2009.06.051. PMID:19683248.

Van Loon, L.R., Glaus, M.A., and Müller, W. 2007. Anion exclusion effects in compacted bentonites: towards a better understanding of anion diffusion. Applied Geochemistry, **22**(11): 2536–2552. doi:10.1016/j.apgeochem.2007.07.008.

Viola, R., Tuller, M., Or, D., and Drasdis, J. 2005. Microstructure of clay-sand mixtures at different hydration states. *In* Proceedings of the International Symposium on Advanced Experimental Unsaturated Soil Mechanics, Trento, Italy, 27–29 June 2005. *Edited by* A. Tarantino, E. Romero, and Y.J. Cui. Taylor & Francis Group, London, UK. pp. 437–442.

Yaroshchuk, A.E. 1995. Osmosis and reverse osmosis in fine-porous charged diaphragms and membranes. Advances in Colloid and Interface Science, **60**(1–2): 1–93. doi:10.1016/0001-8686(95)00246-M.